

Reconciling Semiclassical and Bohmian Mechanics: V. Wavepacket Dynamics

Bill Poirier

*Department of Chemistry and Biochemistry, and Department of Physics,
Texas Tech University, Box 41061, Lubbock, Texas 79409-1061**

In previous articles [J. Chem. Phys. **121** 4501 (2004), J. Chem. Phys. **124** 034115 (2006), J. Chem. Phys. **124** 034116 (2006), J. Phys. Chem. A **111** 10400 (2007)] a bipolar counter-propagating wave decomposition, $\Psi = \Psi_+ + \Psi_-$, was presented for stationary states Ψ of the one-dimensional Schrödinger equation, such that the components Ψ_{\pm} approach their semiclassical WKB analogs in the large action limit. The corresponding bipolar quantum trajectories are classical-like and well-behaved, even when Ψ has many nodes, or is wildly oscillatory. In this paper, the method is generalized for time-dependent wavepacket dynamics applications, and applied to several benchmark problems, including multisurface systems with nonadiabatic coupling.

I. INTRODUCTION

Trajectory interpretations of quantum mechanics have existed since the beginning of the quantum theory—even predating the Schrödinger equation itself. Indeed, one such approach survives today in the form of the Jeffrey-Wentzel-Kramers-Brillouin (JWKB) approximation, or more generally, semiclassical mechanics.^{1,2,3} In this approach, a time-evolving quantum wavepacket is treated as a statistical ensemble of classical trajectories that “carry” approximate quantum information, i.e. complex amplitudes. In the early 1950s, hearkening back to the earlier pioneers, D. Bohm and coworkers developed a conceptually similar trajectory interpretation of the *exact* quantum theory,^{4,5,6} introducing the so-called “quantum potential” to guide the resultant quantum trajectory dynamics. In the intervening years, quantum trajectory methods (QTM)s have been used “analytically”—to provide insight into solved time-dependent quantum wavepacket propagation problems^{7,8,9,10}—and more recently, as a “synthetic” tool—to actually solve the time-dependent Schrödinger equation (TDSE) itself.^{11,12,13,14,15,16,17,18,19} Note that in this paper, “QTM” refers to the original quantum trajectory method based on standard Bohmian mechanics, as developed by Wyatt and coworkers,¹¹ *as well as* the various offshoots and approximations that have developed in the intervening years.

The standard Bohmian formulation uses an amplitude-phase decomposition of the wavefunction, ψ , which in one dimension (1D) takes the form

$$\psi(x, t) = R(x, t)e^{iS(x, t)/\hbar}. \quad (1)$$

This representation has been called “unipolar,”¹¹ because the field functions, $R(x, t)$ and $S(x, t)$, are single-valued at all positions, x , and times, t . The field functions, and the resultant quantum trajectories, are generally smooth and classical-like—provided the true potential, $V(x)$, is slowly-varying, *and* $\psi(x, t)$ exhibits no interference. However, interference introduces non-classical-like oscillations in $R(x, t)$ and $S(x, t)$, which in turn lead to severe numerical difficulties for QTM calculations—

collectively referred to as “the node problem.”^{11,16} Despite substantial progress,^{20,21,22,23} the node problem continues to be the most formidable roadblock impeding the progress of QTM’s as a general and robust tool for exact quantum scattering applications.

As a promising remedy to the node problem, this paper is the fifth in a series^{24,25,26,27} exploring the use of *bipolar* decompositions of the wavefunction, i.e.

$$\psi = \psi_+ + \psi_-, \quad (2)$$

such that the quantum trajectories associated with the bipolar wavefunction components, $\psi_{\pm}(x, t)$, are well-behaved and classical-like, even when the unipolar quantum trajectories associated with $\psi(x, t)$ itself are not—e.g., when $\psi(x, t)$ exhibits interference. In fact, by generalizing Bohmian mechanics for multipolar decompositions such as Eq. (2) above, it becomes possible to achieve *classical correspondence*—i.e., trajectories and field functions that approach their classical counterparts in the classical limit of large mass, energy, and/or action—which is not in general possible for any unipolar Bohmian treatment.

Most QTM papers found in the literature concern themselves with time-dependent localized wavepacket dynamics, as indeed, is also true of this fifth paper in the bipolar series. However, this paper represents a stark departure from the previous four, all of which pertain to stationary solutions of the the time-*independent* Schrödinger equation—albeit obtained in a pseudo-time-dependent manner using delocalized counter-propagating wave components. For 1D stationary states, the two $\psi_{\pm}(x, t)$ components correspond to approximate semiclassical analogs,^{2,3} of which there are always two at every classically-allowed point in space and time—thus justifying a bipolar QTM treatment in this context. If there are classical turning points demarcating classically allowed and forbidden regions, these are known *a priori*, and do not change over time.

In contrast, the semiclassical treatment of localized *wavepacket* dynamics, even in 1D, is considerably more complicated than for stationary states—rendering it far more difficult to arrive at a suitable QTM analog. In par-

particular, the time-evolving semiclassical field functions can become multivalued over regions of x and t in a highly non-trivial way, due to caustics that form, move, and then disappear over time.¹ The appropriate number of semiclassical components can become one, two, or even three or more, and in any case, varies nontrivially over x and t . The formation of caustics, in turn, is due to the crossing of neighboring classical trajectories belonging to a semiclassical wavepacket ensemble. In stark contrast are quantum trajectories, which, for a single component, may *never* cross—implying single-valuedness for all x and t , and evidently greatly complicating the task of achieving classical correspondence.

Let us imagine, for instance, that at the initial time, t_0 , $\psi(x, t_0)$ is taken to be of the unipolar Eq. (1) form. Though initially single-valued, $\psi(x, t)$ may, at later t , become multivalued over certain regions of x , under a semiclassical treatment. However, since an ensemble of *quantum* trajectories does not develop caustics, how then is a QTM to become similarly multivalued? This fundamental difficulty persists even under the usual allowance that quantum and semiclassical wavefunctions are equivalent only to $\mathcal{O}(\hbar)$. In fact, it raises the following, purely semiclassical conundrum, which to the author’s best knowledge, has not been previously addressed: if $\psi(x, t)$ can become multivalued at *later* t , why should it never be considered so at $t = t_0$? One practical reason is that the $\mathcal{O}(\hbar)$ uniqueness of the semiclassical representation would be compromised, making it unclear how to proceed. This answer is not satisfying in any formal sense; yet indeed, semiclassical theory treats the same Gaussian wavefunction as *single-valued* if interpreted in a wavepacket context, or *double-valued* if regarded as a harmonic oscillator ground state.

With regard to QTM wavepacket dynamics, the multivalued problem described above can in principle be addressed in a variety of ways. One simple strategy would be to actually use classical trajectories for the dynamics—not approximately, as in semiclassical theories, but rather, with *exact* propagation of the (complex-valued) quantum amplitudes, $R(x, t)$. This approach can be regarded as an arbitrary Lagrangian-Eulerian (ALE) method,^{11,21,22} modified to allow for the formation of caustics and multivalued fields. Note that probability is no longer conserved along trajectories—and indeed, must approach zero at the caustics, in order to avoid infinite probability density. In practice, this condition itself causes numerical instabilities, and in any case would be unfeasible to implement for large systems.²⁸

Alternatively—and seemingly contrary to semiclassical behavior—one might opt to adhere strictly to a globally bipolar decomposition of the Eq. (2) form, in order to facilitate comparison with the bipolar stationary state theories of papers I–IV in the series.^{24,25,26,27} Even in this relatively restricted context, however, the “correct” bipolar wavepacket generalization is not necessarily obvious. In the previous work, for instance, both of the ψ_+ and ψ_- field functions are symmetric for station-

ary bound states,²⁴ whereas only S is symmetric [i.e., $S_-(x) = -S_+(x)$] for the more general case of stationary scattering states.^{25,26} For bipolar wavepacket dynamics, *neither* field function provides us with simplifying symmetry; moreover, we evidently have no direct recourse to semiclassical mechanics, which was previously relied upon as a guide.

One way to state the problem is as follows: a complete specification of the bipolar wavepacket dynamics generally requires *four* independent real-valued time-evolution equations. Two of these are automatically provided by the TDSE, but how are the remaining two to be chosen? One promising avenue, which we have explored considerably,²⁹ is to adopt the combined flux continuity condition^{26,27,30} [Eq. (17)] as the third equation. In fact, if *imaginary* flux is considered,³¹ the fourth and final equation can also be obtained. Unfortunately, these equations do not provide satisfactory results, in that over time, the individual $\psi_{\pm}(x, t)$ components themselves develop interference oscillations and nodes—thus defeating the purpose of a bipolar expansion. More flexibility can be obtained by dropping the imaginary flux continuity condition, but to date, all such efforts have also been unsuccessful²⁹—either due to $\psi_{\pm}(x, t)$ interference, or other equally unsatisfactory behaviors (Sec. II C).

Ultimately, the most successful bipolar wavepacket generalization scheme we have considered has also proven to be one of the most conceptually straightforward—i.e., to expand $\psi(x, t)$ as a superposition of stationary state solutions, whose + and – components are then used to determine the wavepacket $\psi_{\pm}(x, t)$ via linear superposition. The idea is simple, but the theoretical development is somewhat involved. In any event, this approach, which will serve as the focus of this paper, leads to a node-free, and otherwise remarkably well-behaved Eq. (2) decomposition—and moreover, turns out to satisfy classical correspondence after all. It also leads to time-evolution equations that are practicable for numerical implementation. Note that bipolar quantum trajectory formulations for the TDSE have been considered previously by other authors,³² albeit not in a manner designed to solve the interference/node problem.

The remainder of this paper is organized as follows. Sec. II first presents the requisite background of the bipolar theory for stationary scattering states (Sec. II A), followed by a derivation of the new wavepacket time-evolution equations for asymptotically symmetric potentials (Sec. II B). Additional properties of the resultant $\psi_{\pm}(x, t)$ component wavepacket dynamics are described in Sec. II C. Generalizations for asymptotically asymmetric and multisurface applications are then provided in Secs. II D and II E, respectively. Results and discussion, for benchmark applications of each type described above, are then presented in Sec. III. Finally, a summary and concluding remarks are given in Sec. IV.

II. THEORY

A. Background

Consider the two bipolar components, $\phi_{\pm}^E(x)$, associated with a 1D stationary scattering state solution of the Schrödinger equation, $\phi^E(x) = \phi_+^E(x) + \phi_-^E(x)$, with energy, E , and left-incident boundary conditions. The solution components, $\phi_{\pm}^E(x)$, are exact quantum analogs of a type of semiclassical JWKB approximation resulting from the “generalized Fröman” approach.^{2,26,27,30} Note that for the remainder of this paper, ϕ is used in the context of stationary state wavefunctions, whereas ψ is reserved for localized wavepacket dynamics. The solution components $\phi_{\pm}^E(x)$ behave as (right/left) traveling plane waves in both asymptotes. As x sweeps through the potential interaction region, the solution component $\phi_+^E(x)$ varies smoothly from incident to transmitted wave, whereas $\phi_-^E(x)$ varies smoothly from reflected wave to zero.

In several previous articles,^{25,26,27,30} an extremely accurate, efficient, and robust 1D numerical algorithm was developed for computing $\phi_{\pm}^E(x)$, and thus $\phi^E(x)$. The algorithm is a time-dependent relaxation method, for which the initial $\phi^E = \phi_+^E$ is a plane wave. Over time, a reflected wave, $\phi_-^E(x, t)$, comes into being through interaction region coupling due to the potential energy, and eventually, $\phi^E(x, t)$ relaxes to the true stationary scattering solution.

From Ref. 26 Eq. (12), the $\phi_{\pm}^E(x, t)$ time-evolution equations are

$$\frac{\partial \phi_{\pm}^E}{\partial t} = \mp \frac{p}{m} \phi_{\pm}^{E'} + \frac{i}{\hbar} (E - V) \phi_{\pm}^E - \frac{i}{\hbar} V \phi_{\mp}^E, \quad (3)$$

where primes denote spatial differentiation, m is the mass, $p = \sqrt{2mE}$ is the magnitude of the asymptotic momentum, and asymptotically symmetric potentials are presumed [$V(x) \rightarrow 0$ as $x \rightarrow \pm\infty$]. The initial value conditions are given by

$$\phi_+^{E0}(x) = \phi_+^E(x, t_0) = \exp\left[\frac{ipx}{\hbar} - \frac{iEt_0}{\hbar}\right] \quad (4)$$

$$\phi_-^{E0}(x) = \phi_-^E(x, t_0) = 0,$$

where $t = t_0 \rightarrow -\infty$ is the initial time. At the left and right coordinate limits, i.e. $x = x_L \rightarrow -\infty$ and $x = x_R \rightarrow +\infty$, respectively, the boundary conditions are:

$$\phi_+^E(x_L, t) = \exp\left[\frac{ipx_L}{\hbar} - \frac{iEt}{\hbar}\right] \quad (5)$$

$$\phi_-^E(x_R, t) = 0$$

In general, Eq. (3) does *not* satisfy the TDSE, in that $(\partial \phi^E / \partial t) \neq -(i/\hbar) \hat{H} \phi^E$ for all times t , where \hat{H} is the usual Schrödinger equation Hamiltonian. This is consistent with the interpretation of this approach as a

“revelatory” or “relaxation” method,^{25,26,30} but implies that Eq. (3) itself cannot be used as a basis for deriving wavepacket time-evolution equations, for which the TDSE must be satisfied at all t .

B. Wavepacket time-evolution equations

We therefore consider the asymptotically large time limit, $t \rightarrow +\infty$, in which Eq. (3) not only satisfies the TDSE, but relaxes to the exact stationary solution, so that

$$\frac{\partial \phi^E}{\partial t} = -\frac{i}{\hbar} E \phi^E \quad \text{and} \quad \frac{\partial \phi_{\pm}^E}{\partial t} = -\frac{i}{\hbar} E \phi_{\pm}^E \quad \text{as } t \rightarrow +\infty. \quad (6)$$

Substituting Eq. (6) into Eq. (3) and rearranging yields the following time-independent expressions for the spatial derivatives of the solution ($t \rightarrow +\infty$) $\phi_{\pm}^E(x)$:

$$\phi_{\pm}^{E'} = \pm \frac{i}{\hbar} p \phi_{\pm}^E \mp \frac{i}{\hbar} \left(\frac{m}{p}\right) V (\phi_+^E + \phi_-^E). \quad (7)$$

Equation (7) above is consistent with Ref. 30 Eq. (12), with $v = p/m = \sqrt{2E/m}$. Differentiating Eq. (7) with respect to x , and then using Eq. (7) to substitute for $\phi_{\pm}^{E'}$ in the resulting right hand side yields:

$$\phi_{\pm}^{E''} = -\frac{2m}{\hbar^2} (E - V) \phi_{\pm}^E \mp \frac{i}{\hbar} \left(\frac{m}{p}\right) V' (\phi_+^E + \phi_-^E). \quad (8)$$

Equation 8 can then be used to obtain

$$\hat{H} \phi_{\pm}^E = E \phi_{\pm}^E \pm \frac{i\hbar}{2p} V' (\phi_+^E + \phi_-^E). \quad (9)$$

Substituting Eq. (6) for $E \phi_{\pm}^E$ above then results in the following, new time-evolution equations:

$$\frac{\partial \phi_{\pm}^E}{\partial t} = -\frac{i}{\hbar} \hat{H} \phi_{\pm}^E \mp \frac{V'}{2p} (\phi_+^E + \phi_-^E) \quad (10)$$

A subtle shift has occurred in the transformation from Eq. (3) to Eq. (10). First, the latter manifestly satisfies the TDSE at *all* times t . Second, what constitutes the coupling contribution (i.e. the last term) in Eq. (3) is *not* equivalent to that of Eq. (10). Most strikingly, the latter coupling is proportional to V' rather than to V itself. This implies that the coupling vanishes in both of the coordinate asymptotic limits, x_L and x_R , *even* when $V(x)$ is not taken to be asymptotically symmetric. This represents quite an improvement over Eq. (3), which cannot be applied to asymmetric potentials because there is asymptotic coupling in at least one coordinate limit.^{26,30} Although Eq. (10) can be used with asymptotically asymmetric potentials, there are nontrivial ramifications for wavepacket dynamics (Sec. IID). The final, and perhaps most important, observation that will be made regarding the coupling contribution to Eq. (10) is that it is *directly*

proportional to the JWKB quantity denoting the classical limit—i.e., $|\lambda V'|$, where $\lambda = 2\pi\hbar/p$ is the de Broglie wavelength.³³ In particular, the classical limit is obtained when $|\lambda V'| \ll p^2/2m$ —i.e., $(V'/p) \rightarrow 0$. According to Eq. (10), the coupling *vanishes* in the classical limit, in which the ϕ_{\pm}^E themselves approach Schrödinger equation solutions. In this manner, classical correspondence is established for the new time-evolution equations.

All of the above still refers to delocalized left-incident stationary scattering states ϕ^E , at definite energies E . For every positive E value, the methodology uniquely determines a corresponding ϕ^E and ϕ_{\pm}^E . In generalizing for (left-incident) localized wavepacket dynamics, an eminently sensible strategy is to decompose the wavepacket ψ as an orthonormal expansion in the stationary states ϕ^E —an expansion which, in turn, is applied to the ϕ_{\pm}^E components themselves, to uniquely determine ψ_{\pm} and the Eq. (2) bipolar decomposition. Thus,

$$\begin{aligned}\psi(x, t) &= \int_0^{\infty} a(E)\phi^E(x, t) dE \quad \text{and} \quad (11) \\ \psi_{\pm}(x, t) &= \int_0^{\infty} a(E)\phi_{\pm}^E(x, t) dE.\end{aligned}$$

In principle, the above equations enable $\psi_{\pm}(x, t)$ to be completely determined—provided the initial wavepacket, $\psi^0(x) = \psi(x, t_0)$, is specified, and all of the solution $\phi_{\pm}^E(x, t)$'s are known *a priori*. In practice, the latter requirement defeats the purpose of doing localized wavepacket dynamics—i.e., to avoid explicit calculation of the delocalized ϕ^E states.

Consequently, we apply the Eq. (11) expansion to both sides of Eq. (10), in order to directly derive time-evolution equations for $\psi_{\pm}(x, t)$. We require that the explicit integrations over dE be tractable, so that ϕ^E and ϕ_{\pm}^E not appear explicitly in the final results for $\partial\psi_{\pm}/\partial t$. This in turn requires that the right-hand-side of Eq. (10) exhibit no explicit dependence on E or p , which—due to the coupling term—is seen not to be satisfied. To make progress, we use the identity,

$$\phi^{E'} = \frac{ip}{\hbar} (\phi_+^E - \phi_-^E), \quad (12)$$

obtained from Ref. 26 Eq. (9), or from Ref. 30 Eq. (11), or by using Eq. (7) to add $\phi_+^{E'} + \phi_-^{E'}$. Substituting the integral of Eq. (12) with respect to x into Eq. (10) then yields

$$\frac{\partial\phi_{\pm}^E}{\partial t} = -\frac{i}{\hbar} \left[\hat{H}\phi_{\pm}^E \pm \frac{V'}{2} (\Phi_+^E - \Phi_-^E) \right], (13)$$

$$\text{where } \Phi_{\pm}^E(x) = \int_{-\infty}^x \phi_{\pm}^E(x') dx',$$

apart from a term proportional to $\phi_{\pm}^E(x \rightarrow -\infty)$ that vanishes when integrated over E via Eq. (11) (Dirichlet wavepacket boundary conditions, Sec. III). Since Eq. (13) above has no explicit dependence on E or p , applying the Eq. (11) expansion to Eq. (13) leads at once

to the following wavepacket time-evolution equations:

$$\begin{aligned}\frac{\partial\psi_{\pm}}{\partial t} &= -\frac{i}{\hbar} \left[\hat{H}\psi_{\pm} \pm \frac{V'}{2} (\Psi_+ - \Psi_-) \right], (14) \\ \text{where } \Psi_{\pm}(x) &= \int_{-\infty}^x \psi_{\pm}(x') dx' \quad (15)\end{aligned}$$

Equation (14) can be directly integrated over time, to determine the dynamics of the bipolar wavepacket components, $\psi_{\pm}(x, t)$. In addition to the usual TDSE Hamiltonian contribution, Eq. (14) includes a coupling contribution that is proportional to V' (and independent of mass). As in the case of Eq. (13), this implies that the asymptotic $x \rightarrow \pm\infty$ coupling vanishes, even for asymmetric potentials. Since $V(x)$ also vanishes asymptotically, we thus find that $\psi_{\pm}(x \rightarrow \pm\infty, t)$ evolves under free-particle propagation. Note that throughout the x coordinate range, the ψ_{\pm} coupling terms are equal and opposite, so that $(\partial\psi/\partial t) = -(i/\hbar)\hat{H}\psi$. Thus, Eq. (14) satisfies the TDSE at all t .

C. Additional properties

Having defined a set of wavepacket time-evolution equations [Eq. (14)], we next consider whether these give rise to well-behaved $\psi_{\pm}(x, t)$ components at all x and t . In general, a great range of behaviors are possible for nonstationary state dynamics in 1D, many of which are undesirable. We therefore first stipulate that—apart from exhibiting interference— $\psi(x, t)$ itself be well-behaved. By this we mean that $\psi(x, t)$ is normalized to unity and well-localized at all times t , consisting of a single left-incident wavepacket at the initial time $t = t_0$, and of well-separated left- and right-moving reflected and transmitted branches, respectively, at the final time $t = t_f \rightarrow +\infty$. Under these assumptions for the $\psi(x, t)$ wavepacket dynamics, we define well-behaved *components*, $\psi_{\pm}(x, t)$, as those that satisfy the following three conditions:

- *Condition 1:* Perfect asymptotic separation at t_0 and t_f .
- *Condition 2:* Well-localized $\psi_{\pm}(x, t)$ and $\Psi_{\pm}(x, t)$ at all t .
- *Condition 3:* Node-free components, $\psi_{\pm}(x, t)$, at all t .

Condition 1. means that the initial left-incident wavepacket consists solely of ψ_+ —i.e., $\psi_+^0(x) = \psi^0(x) = \psi(x, t_0)$, and $\psi_-^0(x) = 0$. It also means that at the asymptotically large final time t_f , $\psi_+^f(x) = \psi_+(x, t_f)$ becomes the right-moving transmitted branch of $\psi^f(x) = \psi(x, t_f)$, and $\psi_-^f(x) = \psi_-(x, t_f)$ becomes the left-moving reflected branch. Condition 2. is straightforward, and absolutely

essential, e.g., for multidimensional generalizations. Condition 3. is expected to hold at *all* t —particularly intermediate times, where $\psi(x, t)$ itself may exhibit substantial interference and/or nodes.

For the remainder of this subsection, asymptotically symmetric potentials are presumed, as defined in Sec. II A. At the initial time t_0 , the incident wavepacket is localized far to the left of the potential interaction region, so that $V(x)$ is effectively zero, and the Eq. (5) plane wave boundary condition accurately describes $\phi_{\pm}^E(x, t)$ —over the whole asymptotic region where $|\psi^0(x)|^2$ is significant. Thus, the initial Eq. (11) stationary state expansion is essentially *identical to a Fourier expansion*—or equivalently, the momentum-space representation, $\tilde{\psi}^0(p)$. Through the identification $p = \sqrt{2mE}$, we find that only the $p > 0$ states contribute in the Eq. (11) expansion for $\psi_{\pm}^0(x)$; the $p \leq 0$ states give rise to a left-moving contribution, which is presumed to be zero at $t = t_0$. Condition 1. thus requires that the negative momentum contribution to $\psi^0(x)$ be vanishingly small, i.e.

$$\int_{-\infty}^0 |\tilde{\psi}^0(p)|^2 dp \rightarrow 0. \quad (16)$$

This is a very reasonable requirement to impose on $\psi^0(x)$, for it implies that the initial wavepacket is completely incident upon the scattering potential center.

At the final time t_f , the $a(E)$ expansion coefficients from Eq. (11) are identical to their initial values at t_0 . Moreover, the reflected and transmitted wavepacket branches are localized far to the left and right, respectively, of the interaction region, so that once again, the $\phi^E(x, t)$ are effectively plane waves.^{26,30} However, these asymptotic plane waves are no longer characterized by the standard unit normalization of Eq. (5), but must instead be weighted by the E -dependent reflection and transmission amplitudes, $R(E)$ and $T(E)$, when determining the Fourier components, $\tilde{\psi}^f(p)$. Note that since $\phi_{-}^E(x_R, t) = 0$ [Eq. (5)], there can be no ψ_{-} component in the right asymptote, implying that the right-moving transmitted branch at t_f must consist only of a $\psi_{+}^f(x)$ contribution. Similar arguments can be used to demonstrate that the left-moving reflected branch at t_f must consist only of $\psi_{-}^f(x)$. We thus find that Condition 1. above is formally satisfied at both t_0 and t_f .

Regarding Condition 2., here again we make use of Eq. (16). If Eq. (16) were *not* satisfied, then $\tilde{\psi}(p = 0, t)$ would in general be nonzero. Since $\Psi(x_R, t) = \sqrt{2\pi\hbar}\tilde{\psi}(p = 0, t)$ [from Eq. (15)], the right-asymptotic value of $\Psi(x_R, t)$ would approach a constant (in x), nonzero value. Thus, $\Psi(x, t)$ would be *delocalized*—even if $\psi(x, t)$ itself were localized, as it is initially. Over time, moreover, due to the coupling term in Eq. (14), the $\psi_{\pm}(x, t)$ would themselves eventually become delocalized, even if $\psi(x, t)$ itself were not—clearly, an untenable situation, in violation of Condition 2. Conversely to the above scenario, the fact that Eq. (16) is true implies that

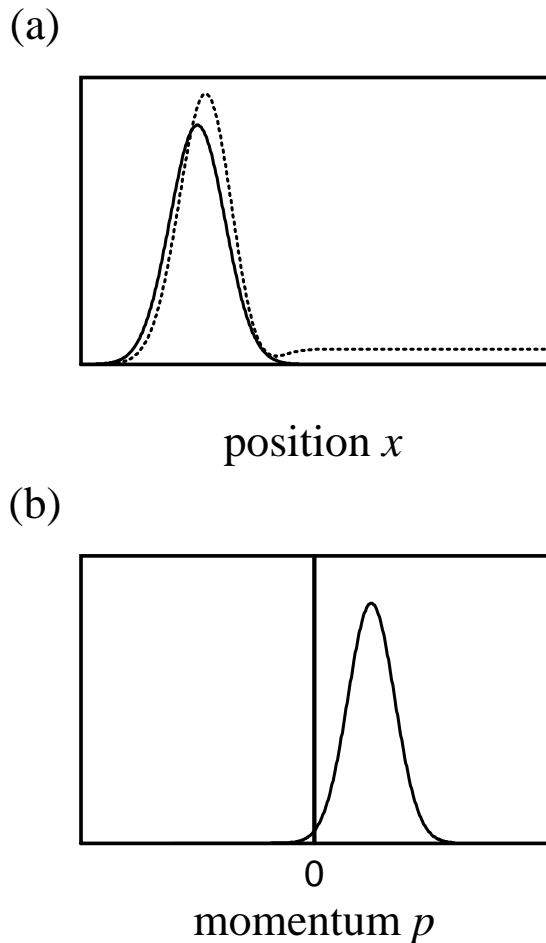


FIG. 1: Schematic indicating properties of initial wavepacket, ψ^0 : (a) position space; (b) momentum space. The solid line in (a) represents $\rho^0(x) = |\psi^0(x)|^2$, the initial wavepacket density, taken to be a Gaussian centered far to the left of the interaction region. The dotted line in (a) represents $|\Psi^0(x)|^2$, where $\Psi(x) = \int_{-\infty}^x \psi(x') dx'$, as per Eq. (15). Note that $\Psi(x)$ is *not* localized, owing to the small constant-valued tail that extends towards $x = +\infty$. This is because the Fourier transform, $\tilde{\psi}^0(p)$, does not satisfy Eq. (16) perfectly—as seen in (b), a plot of $|\tilde{\psi}^0(p)|^2$.

$\Psi_{\pm}(x, t)$, and therefore $\psi_{\pm}(x, t)$, are localized—not *only* at asymptotic times, but at *all* times. Thus, Condition 2. is also formally satisfied.

In practice, Eq. (16) is never perfectly satisfied (even in the $t_0 \rightarrow -\infty$ limit), but is only approximately correct, to some desired level of numerical accuracy. The true $\Psi_{\pm}(x, t)$ will have a small delocalized constant-valued tail—extending to the right towards $x \rightarrow \infty$ for the definite integration convention of Eq. (15), as indicated in Fig. 1, but non-vanishing no matter which integration limits are adopted. For reasonable $\tilde{\psi}^0(p)$ distributions however, the magnitude of these tails can easily be made arbitrarily small (and therefore insignificant) simply by shifting to $\tilde{\psi}^0(p - p_0)$ for sufficiently large p_0 .

Finally, we address the all-important Condition 3. Though we can offer no formal proof at present that this condition is always satisfied, it must certainly be true in the classical limit, in which (V'/p) approaches zero. More generally, if Condition 3. is satisfied for the individual ϕ_{\pm}^E components—as has been demonstrated for a great range and variety of test applications^{25,26,27,30}—then it is reasonable to expect this property to also be preserved under the Eq. (11) expansion. In any event, Condition 3. is verified for each of the test cases considered in Sec. III.

On the other hand, one nice property of the ϕ_{\pm}^E under Eq. (3) that is definitely *not* extended to the ψ_{\pm} under Eq. (14) is that of combined flux continuity. In other words, unlike all previous bipolar formulations for stationary state dynamics,^{26,27,30} we find here that

$$\left(\frac{\partial\rho_+}{\partial t} + \frac{\partial\rho_-}{\partial t}\right) \neq -(j_+' + j_-'), \quad (17)$$

where $\rho_{\pm} = |\psi_{\pm}|^2$ are component densities, and $j_{\pm} = \rho_{\pm}(S_{\pm}'/m)$ are component fluxes, defined in the *standard* quantum manner via

$$\psi_{\pm}(x, t) = R_{\pm}(x, t) \exp[iS_{\pm}(x, t)/\hbar]. \quad (18)$$

The appearance of the standard flux in the above expressions represents a departure from the stationary state formalism—for which predetermined classical velocities, $\pm v$, are used rather than (S'_{\pm}/m) —and a move back towards standard Bohmian mechanics.^{5,6,11} On the other hand, the fact that the Eq. (17) combined flux continuity condition is not satisfied might lead one to argue that the (S'_{\pm}/m) velocity field is inappropriate here, and that some other choice—perhaps some nontrivial generalization of the stationary state velocities—would lead to an Eq. (17)-type equality. In fact this is incorrect—for it can be shown (Sec. III A 1) that $\int_{-\infty}^{+\infty} (\rho_+ + \rho_-) dx$ is not conserved over time, implying the Eq. (17) inequality *regardless* of the particular choice of velocity field. In any event, the standard Bohmian velocity field is naturally obtained when Eq. (14) is used to derive time-evolution equations for the component densities:

$$\frac{\partial\rho_{\pm}}{\partial t} = -j_{\pm}' \pm \frac{V'}{\hbar} \text{Im} [\psi_{\pm}^* (\Psi_+ - \Psi_-)], \quad (19)$$

From Eq. (19) above, Eq. (17) is easily obtained. Note that despite the Eq. (17) inequality, $\int_{-\infty}^{+\infty} (\rho_+^0 + \rho_-^0) dx = \int_{-\infty}^{+\infty} (\rho_+^f + \rho_-^f) dx = \int_{-\infty}^{+\infty} \rho dx = 1$, so that globally over time, the $(\rho_+ + \rho_-)$ probability *is* conserved.

D. Asymptotically asymmetric potentials

Our next task is to generalize the previous discussion for the case of asymptotically asymmetric potentials. To be completely general, we allow the left asymptotic value,

$V_L = V(x_L)$, and right asymptotic value, $V_R = V(x_R)$, to be completely arbitrary—i.e., $V_L \neq V_R$, and neither V_L nor V_R need be zero. In this context, it is straightforward to generalize Eq. (3) for *either* of the two asymptotic potential values, but not both simultaneously. Essentially, this is done by adopting $V^{\text{eff}}(x) = V^0$ as the effective potential used to generate classical trajectories,^{26,27,30} where the constant V^0 is chosen to be either $V^0 = V_L$ or $V^0 = V_R$. In either case, for the generalized Eq. (3), i.e.

$$\frac{\partial\phi_{\pm}^E}{\partial t} = \mp \frac{p}{m} \phi_{\pm}^{E'} + \frac{i}{\hbar} (E - V - V^0) \phi_{\pm}^E - \frac{i}{\hbar} (V - V^0) \phi_{\mp}^E \quad (20)$$

[with $p = \sqrt{2m(E - V^0)}$], coupling vanishes in one x asymptote, but not the other.

As explored in previous papers,^{26,30} two natural remedies for the asymptotic coupling dilemma are considered: (1) define a smoothly varying effective potential $V^{\text{eff}}(x)$ such that $V^{\text{eff}}(x_{L/R}) = V_{L/R}$; (2) define a discontinuous transition at an intermediate dividing point x_D , so that $V^{\text{eff}}(x) = V_L + (V_R - V_L)\Theta(x - x_D)$, where $\Theta()$ is the (heaviside) step function. With respect to deriving wavepacket time-evolution equations as per Sec. II B, option (1) poses severe difficulties, in that it is not clear how to recouch the relevant equations³⁰ to avoid explicit dependence on E and/or p . Option (2) on the other hand, is straightforward, as we now demonstrate.

The key property is that Eq. (20)—whether for $V^0 = V_L$, $V^0 = V_R$, or an arbitrary V^0 value—leads to *exactly* the same wavepacket evolution equations as for $V^0 = 0$, i.e., Eq. (14). However, the resultant ψ_{\pm} components are V^0 -dependent. Thus, the $V^0 = V_L$ components $\psi_{L\pm}$, and the $V^0 = V_R$ components $\psi_{R\pm}$, constitute *distinct* bipolar decompositions, each satisfying Eqs. (2) and (14). This can only be true provided the initial (and final) conditions are different, i.e. $\psi_{L\pm}^0 \neq \psi_{R\pm}^0$ and $\psi_{L\pm}^f \neq \psi_{R\pm}^f$, which in turn implies that Condition 1. (Sec. II C) must be false. In fact, we still find that $\psi_{L+}^0(x) = \psi^0(x)$ and $\psi_{L-}^0(x) = 0$, but both $\psi_{R\pm}^0(x) \neq 0$. Similarly, at t_f , the transmitted branch of $\psi^f(x)$ equals $\psi_{R+}^f(x)$ [no $\psi_{R-}^f(x)$ contribution], but when expanded instead in terms of $\psi_{L\pm}^f(x)$, includes nonzero contributions from both. The reflected branch of $\psi^f(x)$ equals $\psi_{L-}^f(x)$.

In accord with option (2) above, it is natural to define a single bipolar decomposition, ψ_{\pm} , that satisfies all three conditions of Sec. II C, by “gluing” together the asymptotic solutions at the dividing point, x_D , as follows:

$$\psi_{\pm}(x, t) = \Theta(x_D - x) \psi_{L\pm}(x, t) + \Theta(x - x_D) \psi_{R\pm}(x, t) \quad (21)$$

Such a procedure is analogous to other dividing surface methods, commonly used in reactive scattering applications.^{34,35} It is not known at present how to time-evolve Eq. (21) directly, i.e. without recourse to separate calculations for $\psi_{L\pm}$ and $\psi_{R\pm}$ over all x and t . However, the latter is straightforward to achieve in practice—requiring, in addition to Eq. (14), only the specific initial conditions $\psi_{R\pm}^0(x)$, which are derived below.

First, in the Eq. (11) expansion, the lower limit of the integration must be replaced with $E_{\min} = \max(V_L, V_R)$, as reactive scattering does not occur at energies below E_{\min} . For $\psi_{L+}^0(x) = \psi^0(x)$, this expansion is still equivalent to a Fourier expansion, except that the minimum allowed (left) momentum value is

$$p_{\min} = \begin{cases} 0 & \text{if } V_R < V_L; \\ \sqrt{2m(V_R - V_L)} & \text{otherwise.} \end{cases} \quad (22)$$

Thus, the upper limit in Eq. (16) must be replaced with p_{\min} rather than 0, in order that Condition 2. be satisfied. In any event, both $\tilde{\psi}^0(p)$, and the $a(E)$ expansion coefficients in Eq. (11), can be computed explicitly from $\psi^0(x)$ via straightforward Fourier transform.

The next step is to relate the $\phi_{R\pm}^E$ decomposition for the stationary state solution, ϕ^E , to the corresponding $\phi_{L\pm}^E$ decomposition. Applying Eq. (7) to $\phi_{R\pm}^E$, and rearranging, we obtain

$$\phi_{R\pm}^E = \frac{1}{2} \left[\phi^E \mp \left(\frac{i\hbar}{p_R} \right) \phi^{E'} \right], \quad (23)$$

where $p_R = \sqrt{2m(E - V_R)}$. For purposes of expanding the initial wavepacket $\psi^0(x) = \psi_{L+}^0(x)$, we can replace ϕ^E in Eq. (23) with ϕ_{L+}^E . Moreover, the x range of interest is restricted to the left asymptote, where the $\phi_{L\pm}^E$ are plane waves of the Eq. (5) form, but with p replaced by $p_L = \sqrt{2m(E - V_L)}$. Making these substitutions in Eq. (23) leads to

$$\phi_{R\pm}^E = \frac{1}{2} [1 \pm p_L/p_R] \phi_{L\pm}^E, \quad (24)$$

from which $\psi_{R\pm}^0(x)$ can be obtained via straightforward inverse Fourier transform. In particular, Eqs. (11) and (24) lead to

$$\begin{aligned} \psi_{R\pm}^0(x) &= \int_{E_{\min}}^{\infty} a(E) \frac{1}{2} \left[1 \pm \sqrt{\frac{E - V_L}{E - V_R}} \right] \\ &\times \exp \left\{ \frac{i}{\hbar} \left[\sqrt{2m(E - V_L)}x - Et_0 \right] \right\} dE. \end{aligned} \quad (25)$$

Similar arguments can be used to justify the other initial and final conditions for $\psi_{L\pm}$ and $\psi_{R\pm}$, as discussed earlier in this subsection.

Using the explicit initial value conditions of Eq. (26), propagation of the $\psi_{R\pm}(x, t)$ thus becomes as straightforward as for $\psi_{L\pm}(x, t)$. Once achieved, Eq. (21) can then be used to construct a bipolar $\psi_{\pm}(x, t)$ decomposition that satisfies *all three* conditions of Sec. II C. On the other hand, from a purely practical standpoint, little harm would result if one were to simply use $\psi_{L\pm}(x, t)$ throughout x and t . The reason is that, unlike Eq. (20), Eq. (14) exhibits no coupling in *either* x asymptote. Thus, at both t_0 and t_f for instance, $\psi_{L\pm}(x, t)$ [and $\psi_{R\pm}(x, t)$] evolve according to free particle propagation, which introduces no nodes or interference. Condition 3.

is therefore satisfied. In practice, this is far more important than Condition 1., which—as discussed above—is not satisfied for the $\psi_{L\pm}^f$ decomposition in the transmitted branch of $\psi^f(x)$.

E. Multisurface generalization

Like the bipolar stationary state theory, the theory of bipolar wavepacket dynamics can also be generalized for 1D multisurface applications. Let f denote the number of electronic states considered. A diabatic-like time-independent matrix Schrödinger equation is presumed, of the form

$$\tilde{H} \cdot \vec{\phi}^E = E \vec{\phi}^E, \quad (26)$$

where $\{\phi_1^E, \phi_2^E, \dots, \phi_f^E\}$ comprise the vector components (associated with each of the f diabatic states) of the nuclear stationary state wavefunction, $\vec{\phi}^E$, and

$$[\tilde{H}]_{i,j} = -\delta_{i,j} \left(\frac{\hbar^2}{2m} \right) \frac{\partial^2}{\partial x^2} + V_{i,j}(x) \quad (27)$$

are the components of the $f \times f$ Hamiltonian operator matrix, \tilde{H} , with $i \leq f$ and $j \leq f$ labeling diabatic states.

The $V_{i,j}(x) = V_{j,i}(x)$ are the diabatic potential energy curves, with the $i \neq j$ case denoting the coupling potentials. In order to ensure that intersurface coupling vanishes in the asymptotic limits (required to obtain asymptotic scattering waves with correct boundary conditions),^{26,27,30} we must have $V_{i \neq j}(x_L) = V_{i \neq j}(x_R) = 0$. However, the asymptotic values for the diagonal potentials, $V_{i,i}(x)$, are allowed to be completely arbitrary, and in particular, need not be symmetric. Left and right asymptotic values are denoted $V_{iL} = V_{i,i}(x_L)$ and $V_{iR} = V_{i,i}(x_R)$, respectively.

As per Sec. II D, rather than work with generic effective potentials $V_i^{\text{eff}}(x)$ that smoothly interpolate between V_{iL} and V_{iR} values,²⁷ we instead choose constant effective potentials, $V^{\text{eff}}(x) = V^0$, with V^0 arbitrary for now. Note that in general, V^0 can be chosen to coincide with at most one of the V_{iL} and V_{iR} , so that we expect no more than one of the $2f$ component asymptotes to manifest perfect asymptotic separation (Condition 1. from Sec. II C).

From Ref. 27, the $\phi_i^E = \phi_{i+}^E + \phi_{i-}^E$ components satisfy

$$\phi_i^{E'} = \frac{i p}{\hbar} (\phi_{i+}^E - \phi_{i-}^E), \quad (28)$$

where $p = \sqrt{2m(E - V^0)}$. By combining Eq. (26) with Eq. (28), we obtain

$$\phi_{i\pm}^{E'} = \pm \frac{i}{\hbar} p \phi_{i\pm}^E \pm \frac{i}{\hbar} \left(\frac{m}{p} \right) V^0 \phi_i^E \mp \frac{i}{\hbar} \left(\frac{m}{p} \right) \sum_{j=1}^f V_{i,j} \phi_j^E, \quad (29)$$

the multisurface generalization of Eq. (7). Note that the *same* constant p is used for all components i , and in both asymptotes x_L and x_R .

By differentiating Eq. (29) with respect to x , and otherwise applying the procedure described in Sec. IIB, we obtain time-evolution equations for the stationary state components,

$$\frac{\partial \phi_{i\pm}^E}{\partial t} = -\frac{i}{\hbar} \sum_{j=1}^f [\tilde{H}]_{i,j} \phi_{j\pm}^E \mp \frac{1}{2p} \sum_{j=1}^f V'_{i,j} \phi_j^E, \quad (30)$$

the multisurface generalization of Eq. (10). Finally, substitution of the integral of Eq. (28) (with respect to x) into Eq. (30), and integration over E via an Eq. (11)-type expansion yields the following multisurface wavepacket time-evolution equations:

$$\frac{\partial \psi_{i\pm}}{\partial t} = -\frac{i}{\hbar} \left[\sum_{j=1}^f [\tilde{H}]_{i,j} \psi_{j\pm} \pm \left(\frac{1}{2} \right) \sum_{j=1}^f V'_{i,j} (\Psi_{j+} - \Psi_{j-}) \right], \quad (31)$$

where

$$\Psi_{j\pm} = \int_{-\infty}^x \psi_{j\pm}(x') dx' \quad (32)$$

Note that Eq. (31) satisfies the multisurface TDSE, in that

$$\frac{\partial \psi_i}{\partial t} = -\frac{i}{\hbar} \left\{ \sum_{j=1}^f [\tilde{H}]_{i,j} \psi_j \right\}. \quad (33)$$

For a given value of V^0 , it is a straightforward matter to propagate all of the $\psi_{i\pm}$ wavefunction components over time, using Eq. (31) in conjunction with initial value conditions discussed below. The resultant $\psi_{i\pm}(x, t)$ will in general satisfy Conditions 2. and 3. from Sec. IIC, but not Condition 1. Note that the particular $\psi_i = \psi_{i+} + \psi_{i-}$ decompositions obtained depend on the value of V^0 , even though the time evolution equations [Eq. (31)] are V^0 -independent. As described in Sec. IID, the V^0 dependence manifests in the initial conditions, $\psi_{i\pm}^0(x)$.

In addition to the conventions and conditions already adopted for “well-behaved” wavepacket dynamics in Sec. IIC, let us further presume for the multisurface case that the initial wavepacket is left-incident on surface $i = 1$. Then, $\psi_{(i>1)\pm}^0(x) = 0$, but $\psi_{1\pm}^0(x)$ depends on V^0 via an Eq. (26)-type expansion (with $\psi_{R\pm}^0$ replaced with $\psi_{1\pm}^0$, V_L replaced with V_{1L} , and V_R replaced with V^0). One natural choice for V^0 is $V^0 = V_{1L}$ itself, leading to $\psi_{1+}^0(x) = \psi_1^0(x)$ and $\psi_{1-}^0(x) = 0$. This choice leads to perfect asymptotic separation (i.e. Condition 1.) for $\psi_{1\pm}(x, t)$ in the left asymptote, but generally not for $\psi_{1\pm}(x, t)$ in the right asymptote, nor for any of the $\psi_{(i>1)\pm}(x, t)$'s in *either* asymptote.

We again reiterate that from a practical numerical perspective, Condition 1. is not required—i.e. perfectly sensible results for all $\psi_{i\pm}(x, t)$ may be obtained using the $V^0 = V_{1L}$ choice above, or any other reasonable V^0 value. On the other hand, if one is determined to have perfect asymptotic separation for both left and right asymptotes for all i , this can also be achieved—via introduction of a dividing point x_D , and the multisurface generalization of Eq. (21). In effect, this would require that up to $2f$ separate calculations be performed, corresponding to all of the distinct possibilities for $V^0 = V_{iL}$ and $V^0 = V_{iR}$. For each of these calculations, Condition 1. is guaranteed for (at least) one ψ_i component in one asymptote, which is then singled out in that particular calculation—e.g., $\psi_{2R+}(x > x_D, t)$, from the $V^0 = V_{2R}$ calculation. Finally, we note that for the asymptotically symmetric special case considered in Ref. 24, where $V_{iL} = V_{iR} = 0$ for all i , then the *single* choice $V^0 = 0$ leads to perfect separation in both asymptotes for *all* components ψ_i .

III. RESULTS

We have applied the bipolar wavepacket time-evolution equations derived in Sec. II to a variety of model 1D applications. The primary goal is to validate numerically that this approach satisfies the three conditions of Sec. IIC, especially Condition 3. Consequently, little attention is paid here to numerical efficiency, and only the simplest algorithms are employed, using Eulerian fixed grids with uniform spacing in x and t . No trajectories or quantum potentials are computed; these will be considered in later papers, that will actually solve the TDSE by synthesizing quantum trajectories “on the fly.”

In this paper, Eqs. (14) and (31) are integrated over time using the standard first-order forward Euler method, with fixed time step size, Δ .³⁶ Eulerian fixed grids are used to discretize the spatial coordinate x , with uniform spacing Δx , and left and right grid edges, x_L and x_R , respectively. Condition 2. from Sec. IIC implies that Dirichlet boundary conditions, $f(x_L) = f(x_R) = 0$, are employed, where $f(x)$ represents any wavefunction component or its spatial integral. The spatial derivatives implicit in the \hat{H} contribution to Eqs. (14) and (31) are evaluated numerically using standard symmetric (two-sided) second-order finite difference.³⁶ The spatial integrations are evaluated using closed Newton-Cotes formulas—specifically, the two-point trapezoidal rule for the second grid point from the left, and the three-point Simpson’s rule for all other interior grid points.³⁶

The initial wavepackets are all taken to be of the standard Gaussian form,

$$\psi^0(x) = \left(\frac{2\gamma}{\pi} \right)^{1/4} \exp[-\gamma(x - x_0)^2] \exp\left(\frac{ip_0 x}{\hbar} \right), \quad (34)$$

from which $\tilde{\psi}^0(p)$ can be determined analytically. In all calculations, the parameters γ and p_0 are chosen such

that the Eq. (16) integral is negligibly small, i.e. comparable to the desired level of numerical accuracy for the calculation, which is 10^{-6} . Similarly, all of the other numerical parameters, Δ , Δx , x_L , x_R , and x_0 , are converged to the same level of accuracy. For the model applications considered here, typical converged parameter values in atomic units are as follows: $\Delta \approx 0.1$; $\Delta x \approx 0.08$; $x_{L/R} = \mp 35$. Unless explicitly stated otherwise, the mass is taken to be $m = 2000$ a.u. Computer animations (.wmv file format) for all of the wavepacket dynamics calculations presented in this paper are available as EPAPS supplements,³⁷ and by direct request from the author.

A. Eckart barrier system

The canonical model scattering system for the asymptotically symmetric special case is the Eckart barrier,^{38,39} defined via

$$V(x) = V_0 \operatorname{sech}(\alpha x)^2, \quad (35)$$

and specification of the parameters V_0 , α , and m .

1. proton-like mass

For the first Eckart application considered here, the parameter values are chosen to be $V_0 = .0024$, $\alpha = 2.5$, and $m = 2000$, respectively, in atomic units. This is similar to what has been called the ‘‘Eckart A’’ system in previous papers.^{26,27,30} In atomic units, the parameters describing the initial Gaussian wavepacket of Eq. (34) are taken to be $\gamma = 0.35$, $x_0 = -7.0$, and $p_0 = \sim 3.28634$ a.u. [Fig. 2(a)]. The p_0 value corresponds to an incident kinetic energy of .0027 a.u., which is slightly above the barrier energy V_0 , so that substantial reflected and transmitted branches of $\psi^f(x)$ are obtained.

The $\psi_{\pm}(x, t)$ components are propagated using Eq. (14), and the numerical methods described above, to a final time $t_{\max} = (t_f - t_0) = 11600$ a.u., where reflected and transmitted branches are found to be well-separated in left and right asymptotic regions, respectively. Fig. 2 shows the resultant wavepacket dynamics for $\psi_{\pm}(x, t)$ and $\psi(x, t)$ at four representative time slices, including $t = t_0 = 0$ and $t = t_f = t_{\max}$. Although only four time slices are presented, the bipolar decomposition has been carefully inspected at all intermediate times (Fig. 3), to ensure that Fig. 2 captures all of the relevant dynamics.

We find that Condition 1., Condition 2., and above all, Condition 3. (from Sec. II C) are indeed well satisfied at all times. Both bipolar components $\psi_{\pm}(x, t)$ are remarkably smooth, localized, non-oscillatory, and Gaussian-like at all times—despite the fact that $\psi(x, t)$ itself displays a substantial amount of interference at intermediate times [dashed curves, Fig. 2(b) and (c)]. In

addition to interference, the proton-like mass is sufficiently small that the wavepacket dynamics also manifest substantial *dispersion*, as well. In fact—apart from a small ‘‘spur’’ that develops on its left side (Sec. III A 2), and the fact that its integrated probability decreases over time—the $\psi_+(x, t)$ evolution resembles that of a *free particle Gaussian wavepacket*, simultaneously translating and dispersing its way through the interaction region, and in the process, smoothly transforming from the incident wavepacket into the transmitted branch of the final wavepacket.

In contrast, the $\psi_-(x, t)$ wavepacket dynamics—though similarly smooth and well-behaved—exhibit somewhat different behavior, due to the different initial value conditions. In particular, the $\psi_-(x, t)$ component is initially zero, but gradually comes into being in the interaction region, as the $\psi_+(x, t)$ wavepacket passes through. The form of the coupling in Eq. (14) all but assures at least this much. In addition, however—and quite unexpectedly—we also find that the $\psi_-(x, t)$ time-evolution undergoes two distinct stages. In the first stage, $\psi_-(x, t)$ *stays in place* in the interaction region, as it grows steadily in magnitude. Once the $\psi_-(x, t)$ integrated probability has grown to roughly the final reflection probability value, the second stage commences, in which $\psi_-(x, t)$ starts dispersing and moving to the left, in roughly the same manner as for a free particle Gaussian. This two-stage behavior—somewhat reminiscent of fruit ripening on a tree, and then breaking free—is clearly evident in Fig. 3, an ‘‘animation plot’’²⁷ of the time-dependent $\rho_{\pm}(x, t)$ densities.

Note that the transition from stage 1 to stage 2 occurs at a time substantially *after* the $\psi_+(x, t)$ peak has passed by that of $\psi_-(x, t)$. The resultant ‘‘time delay’’ is a manifestation of the quantum Goos-Hänchen effect.^{40,41} The present bipolar approach thus provides a means of measuring this effect *directly*. The Goos-Hänchen time-delay effect appears to be closely related to the lack of combined flux continuity discussed in Sec. II C. Note that for this application, the total integrated probability, $\int_{-\infty}^{+\infty} (\rho_+ + \rho_-) dx$, is fairly well conserved over time, dipping down gradually from the initial value of 1 to a minimum value of 0.86, and then increasing to reach the final value of 1 again by the end of the propagation, as required.

2. the ψ_+ ‘‘spur,’’ and its semiclassical interpretation

One very interesting and unexpected feature is the small spur formed on the left side of $\psi_+(x, t)$ at intermediate times. This spur remains behind the main ψ_+ peak, staying in place above the growing ψ_- wavepacket during stage 1., and then moving ‘‘backwards’’ with ψ_- during stage 2 (as is more evident in calculations for parameters other than those used in Sec. III A 1). At a certain point in time, either before or after the start of stage 2., the spur starts to diminish in size, and eventu-

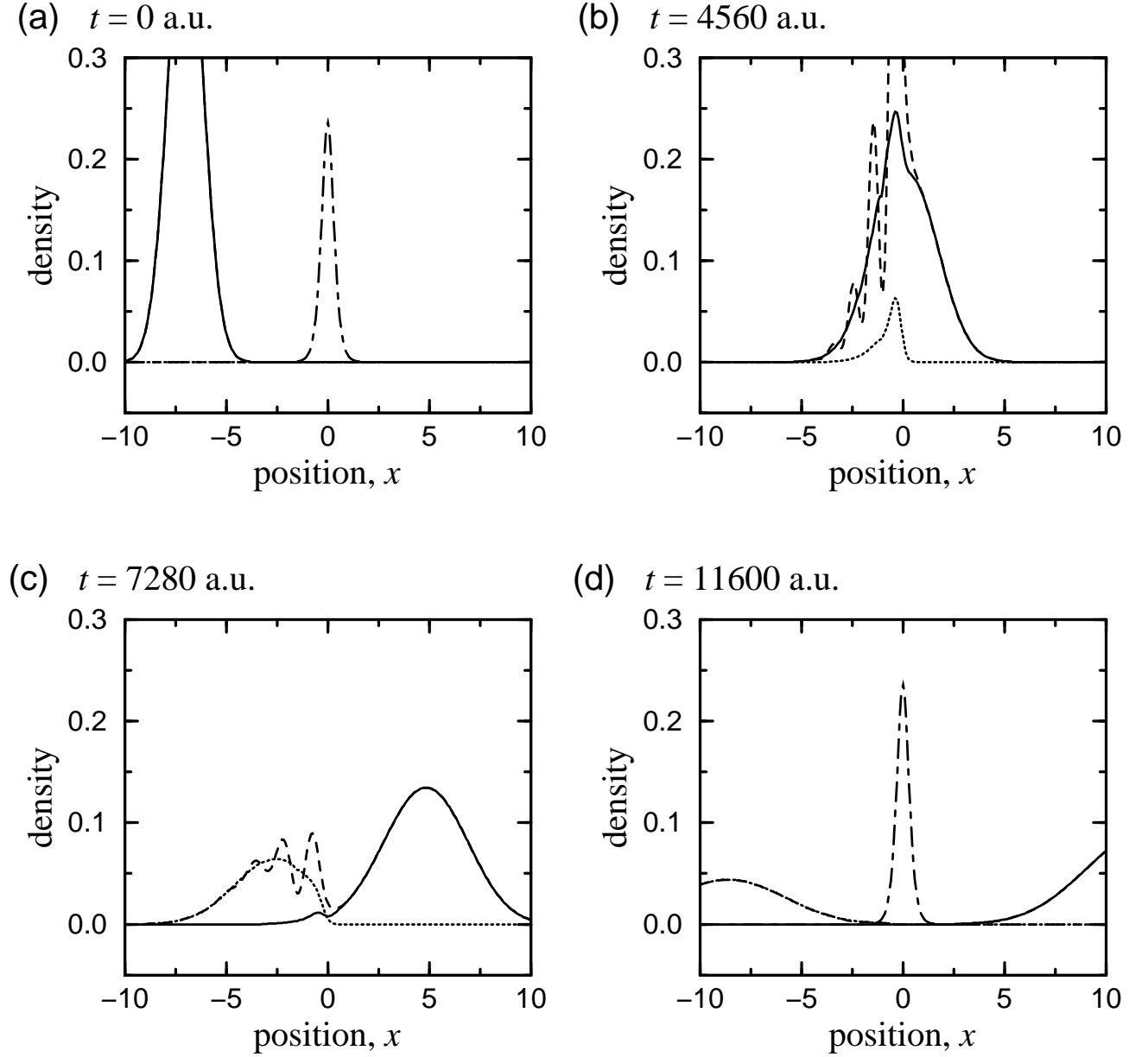


FIG. 2: Wavepacket dynamics for the symmetric Eckart barrier system with $m = 2000$ a.u. Each plot represents a “snapshot” for a specific time, t , as listed (all units are atomic units). Various component wavepacket densities as a function of position are indicated as follows: incident/transmitted, $\rho_+(x) = |\psi_+(x)|^2$, (solid); reflected, $\rho_-(x) = |\psi_-(x)|^2$, (dotted); total, $\rho(x) = |\psi(x)|^2$, (dashed). Initial and final densities, e.g. $\rho^0(x)$ and $\rho^f(x)$, are presented in (a) and (d) respectively, in which the potential energy is also represented (dot-dashed). In (b), the main peak of $\psi_+(x)$ has just passed that of $\psi_-(x)$, though the spur (clearly visible) is forming. The interference is mainly type I, and $\psi_-(x)$ is in stage 1. In (c), $\psi_-(x)$ is in stage 2, and the interference is type II—caused by the $\psi_+(x)$ spur, even though it has dissipated almost completely by this point.

ally dissipates completely. From Fig. 2, the role of the spur is clear—i.e., to bring about interference in the left, or “reflected,” part of $\psi(x, t)$, at intermediate times.

It is well-known that the “reflected” part of $\psi(x, t)$ exhibits nodes and interference to a far greater extent than the transmitted part—indeed, one common strategy in traditional unipolar QTM calculations is to ignore the reflected part altogether, after a certain point in time.¹¹ To some extent, the observed interference in $\psi(x, t)$ is due to

the the incident/transmitted and reflected contributions. However, this cannot be the whole of the story, for the incident/transmitted contribution [main $\psi_+(x, t)$ peak] often passes by, long before the interference goes away completely. Indeed, the so-called “node healing” process may continue even *after* $\psi_-(x, t)$ has started to move away from the interaction region. Eventually though, the nodes will be healed completely—leading to a smooth final $\psi^f(x)$ reflected branch, and causing the $\psi_+(x, t)$ spur

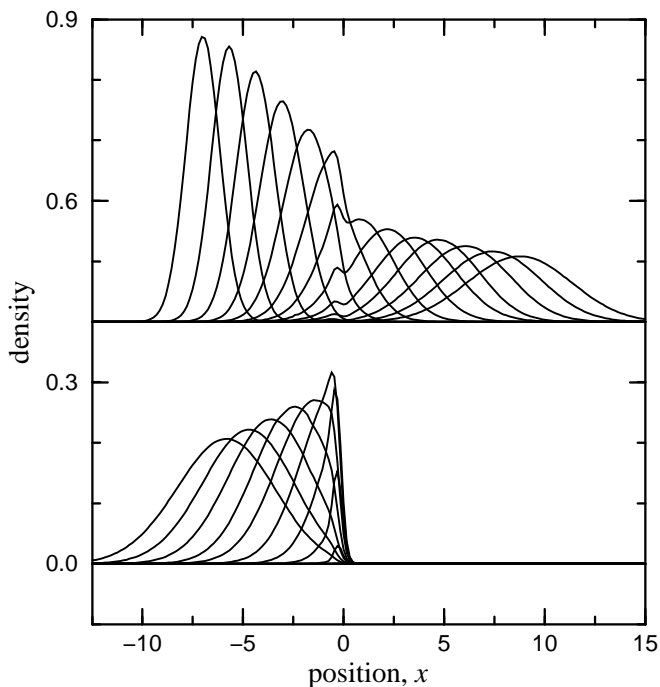


FIG. 3: Component wavepacket densities, $\rho_{\pm}(x, t)$ as a function of position, and for a variety of times, t , for the symmetric Eckart barrier system with $m = 2000$ a.u. The upper family of curves represent $\rho_+(x)$ at different times, whereas the lower family of curves represent $\rho_-(x)$ (magnified by a factor of $4\times$). The motion of the former over time is left-to-right, whereas that of the latter is right-to-left. At intermediate t , a stationary $\rho_+(x)$ spur forms and then dissipates in the interaction region, corresponding with the simultaneous “birth” and stationary growth of $\rho_-(x, t)$. This is “stage 1” of the reflected wavepacket dynamics (Sec. III A 1), represented in the figure by the right-most four $\rho_-(x)$ curves. A sudden transition to stage 2 dynamics is then observed, in which $\rho_-(x)$ moves to the left.

to vanish from existence.

It would thus appear natural to interpret the above as the result of not two, but *three* separate contributions, as considered briefly in Sec. I, each of which is smooth and well-behaved at all times. In particular, the $\psi_-(x, t)$ component is the reflected contribution, the main peak of $\psi_+(x, t)$ is the incident/transmitted contribution, and the $\psi_+(x, t)$ spur—non-zero only at intermediate times—is the third contribution. There are thus two distinct types of interference: type I, between incident/transmitted and reflected contributions, and type II, between spur and reflected contributions. It is quite remarkable that the Eq. (14) decomposition should be generally capable of smoothly disentangling such varied and complex interference patterns—a very delicate balance is evidently required—yet this appears to be the case.

In Fig. 2(c), for instance, one can discern interference in the $\rho(x)$ plot far to the left of the interaction region, where $\rho_+(x)$ itself appears to be vanishingly small. Yet

this tiny $\psi_+(x)$ contribution is very significant, for without it, $\rho(x)$ would equal $\rho_-(x)$, which by visual inspection is clearly false. There is thus a pronounced sensitivity in any Eq. (2) bipolar decomposition—owing ultimately to the square-root relation between ψ and ρ —which in practice, renders it exceedingly difficult to completely disentangle interference effects.

Returning to the idea of a *tripolar* decomposition, we comment that further justification for this interpretation can be provided using semiclassical arguments.²⁸ In particular, consider an Eckart barrier scattering problem for which the initial Gaussian wavepacket is *spreading* (dispersing) at the initial time t_0 [unlike Eq. (34)]. This stipulation is necessary in order that the classical trajectories of the ensemble follow different orbits, so that partial transmission and reflection can be achieved in a semiclassical context. Figure 4 represents the time-evolution of such a classical trajectory ensemble, or “Lagrangian manifold” (LM),^{1,24,25,26,42,43,44,45} in phase space.

The semiclassical LM, though initially single-valued, develops caustics over time, rendering it multivalued at later times. In particular, one caustic (labeled “A” in Fig. 4) forms on the left of the barrier peak, essentially sweeping through all of the individual trajectory turning points, for those classical trajectories with insufficient energy to clear the barrier. For a fairly narrow initial momentum distribution, this caustic will not move very much in x -space, over time. At a given time, those trajectories that have moved through caustic A constitute the reflected branch of the wavepacket, whereas those that have not comprise the incident/transmitted wavepacket. In any event, caustic A is responsible for type I interference.

Let us assume that the leading trajectories of the ensemble have sufficient energy to clear the barrier—thus giving rise to the transmitted branch of the LM at sufficiently large times. Since the LM must be simply connected, there must be a *second* caustic to the left of caustic A (labeled “B”), which allows the LM to double back through the interaction region and connect with the transmitted branch, as indicated in the figure. Caustic B represents the leading edge of the reflected wavepacket, and as such, continually moves to the left. Over time, the connecting thread between B and the transmitted branch gets pulled apart by the separatrix “like taffy,” so that the integrated thread probability becomes vanishingly small. The connecting thread itself therefore corresponds to the ψ_+ spur, giving rise to type II interference, and a *tripolar* LM representation in the “reflected” part of $\psi(x, t)$. The present bipolar approach thus achieves classical correspondence in the classical limit. In addition—as also observed previously in the bipolar treatment of stationary states^{24,25,26,27,30}—it also leads to smooth, classical-like behavior far from the classical limit.

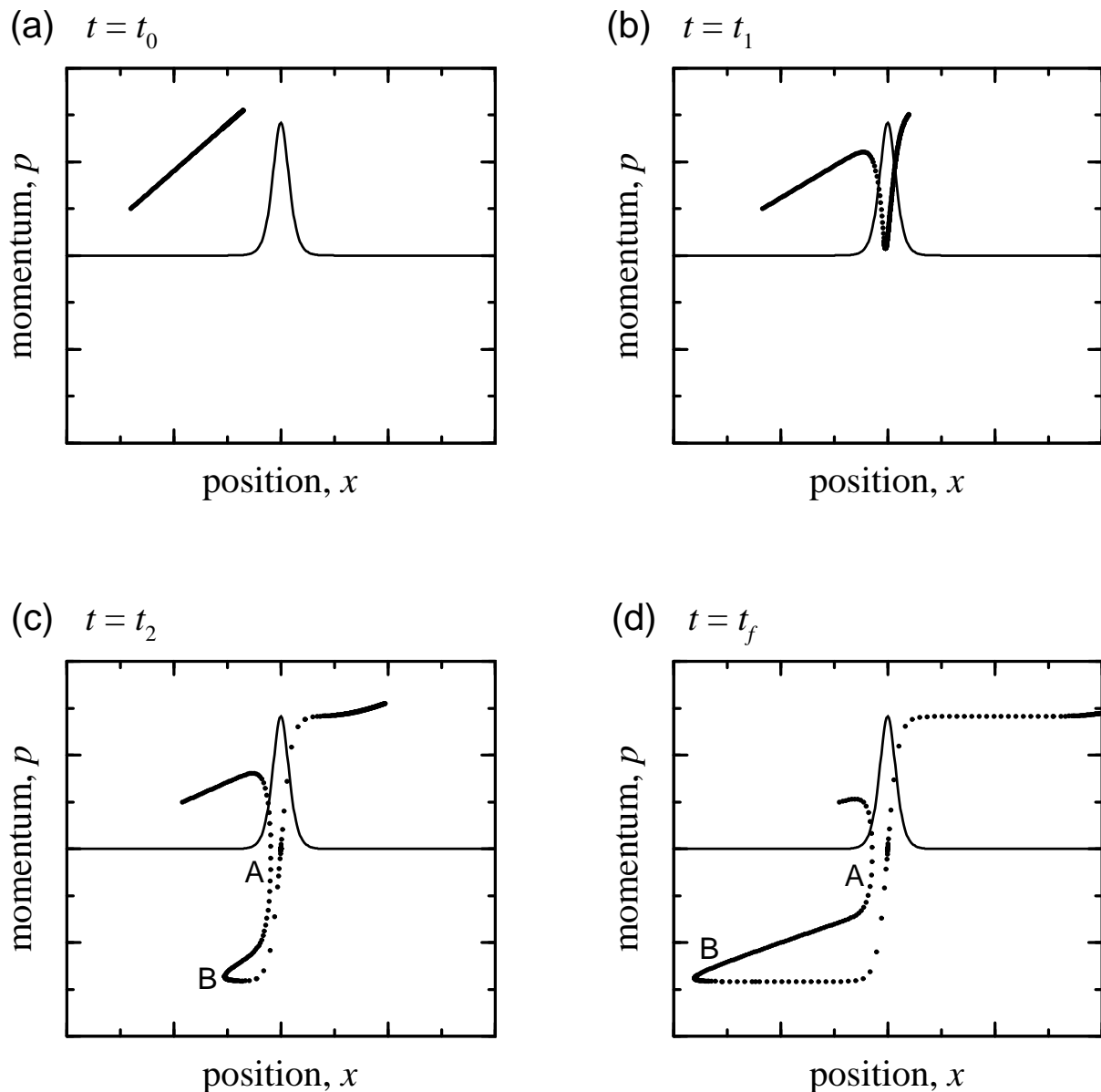


FIG. 4: Semiclassical Lagrangian manifold (LM) dynamics for the symmetric Eckart barrier system. Each plot represents a “snapshot” for a specific time, t . Thin solid curve represents the Eckart potential. One-dimensional array of filled circles represents discrete ensemble of classical trajectories, comprising the LM in phase space at each point in time: (a) the initial $t = t_0$ LM is single-valued with respect to x ; (b) by $t = t_1$, the LM is still single-valued, but is about to form caustics; (c) at a later time $t = t_2$, two caustics have formed, rendering the left side of the LM tripolar; (d) caustic B moves to the left over time.

3. electron mass

The general conclusions discussed in Secs. III A 1 and III A 2 have also been confirmed for a wide variety of other parameter value choices for the Eckart barrier potential [Eq. (35)] and initial wavepacket [Eq. (34)], including deep tunneling applications. In the interest of brevity, we forego additional discussion of most of these additional calculations. However, in light of the final comments in the preceding Sec. III A 2, there is one particular case that merits further attention—i.e., the quan-

tum limit in which $m \rightarrow 0$. To this end, we have performed bipolar wavepacket dynamics calculations for the Eckart system using the *electron* mass $m = 1$, rather than the proton-like $m = 2000$. Even in this extremely non-classical regime, we find that the dynamical characterization of $\psi_{\pm}(x, t)$, as discussed in the preceding subsections still holds true.

In atomic units, the particular parameter values used are as follows: $V_0 = 20$; $\alpha = 1.0$; $m = 1$; $\gamma = 1.0$; $x_0 = -7.5$; $p_0 = \sim 7.74597$. The p_0 value corresponds to an incident kinetic energy of 30 a.u., somewhat above the barrier peak, but leading to substantial reflection and

transmission. Figure 5 shows the resultant wavepacket dynamics for $\psi_{\pm}(x, t)$ and $\psi(x, t)$ at four representative time slices, including $t = t_0 = 0$ and $t = t_f = t_{\max} = 2.5$ a.u. In comparison with Sec. III A 1, the dynamics is of course much faster, and there is substantially less interference, as expected. Another difference is that no $\psi_+(x, t)$ spur is evident, so that the interference appears to be mainly of the type I variety. In other respects, however, the situation is similar to the proton-like mass case—in particular, all three conditions of Sec. II C are clearly satisfied. This system also exhibits a substantial Goos-Hänchen time delay.

B. Barrier ramp system

The barrier ramp scattering system has an asymmetric potential with a barrier. It serves as a generic reaction profile for any direct chemical reaction, and is thus an important benchmark system. The potential functional form consists of an Eckart barrier added to a hyperbolic tangent function, i.e.

$$V(x) = V_0 \operatorname{sech}(\alpha x)^2 + \left(\frac{V_R - V_L}{2} \right) [\tanh(\beta x) + 1], \quad (36)$$

such that the limiting values are $V(x_{L/R}) = V_{L/R}$, as expected. In atomic units, the particular parameter values used for the first barrier ramp calculation are as follows: $V_0 = .0020$; $\alpha = \beta = 2.5$; $V_L = 0$; $V_R = .0008$; $m = 2000$; $\gamma = 0.35$; $x_0 = -7.0$; $p_0 = 4$. These parameters are chosen to correspond to those in Sec. III A 1, except that a larger p_0 value is required, in order that Eq. (16) still be true with an upper limit of p_{\min} rather than 0 (Sec. II D). The p_0 value chosen corresponds to an incident kinetic energy of .004 a.u., which is substantially above the barrier peak of $\sim .0024$ a.u.

As per the discussion in Sec. II D, two separate propagations are performed, using Eq. (14) for two different sets of initial conditions, to a final time $t_{\max} = 9570$ a.u. The first propagation is for the left $\psi_{L\pm}(x, t)$ bipolar decomposition, corresponding to $V^0 = V_L = 0$, for which $\psi_{L+}^0(x) = \psi^0(x)$ and $\psi_{L-}^0(x) = 0$. The second propagation is for the right $\psi_{R\pm}(x, t)$ decomposition, for which the initial value condition is given by the Eq. (26) integration, which is computed numerically using standard Fourier transform methods. The two sets of solutions are then spliced together discontinuously via Eq. (21) at the dividing point, $x_D = 0$.

Figure 6 shows the resultant wavepacket dynamics at four representative time slices. The behavior is exactly as predicted in Sec. II D, and otherwise comparable to that of Sec. III A 1—except that the reflected branch is smaller, owing to the larger initial p_0 value. In particular, all three conditions of Sec. II C are satisfied, and the bipolar components $\psi_{\pm}(x, t)$ are smooth and well-behaved—except of course for the discontinuous join at $x = x_D$, most evident in the $\rho_+(x)$ plot of Fig. 6(b). The

$\psi_{\pm}(x, t)$ are also interference-free, though $\psi(x, t)$ itself exhibits substantial interference at intermediate times, as in Sec. III A 1. Though difficult to discern directly from the figure, $\psi_{L+}(x, t)$ forms a small spur, which serves to heal the nodes in the reflected part of $\psi(x, t)$, as observed for the Eckart barrier, and discussed in Sec. III A 2.

As an alternative to the above asymptotic joining procedure, Sec. II D also suggests simply working with the $\psi_{L\pm}(x, t)$ solutions throughout all x and t . The resultant wavepacket dynamics are still anticipated to be smooth and well-behaved everywhere, though Condition 1. will no longer be satisfied in the $(x > x_D, t_f)$ limit. As an added benefit, moreover, it should be possible to work with initial wavepackets with substantial $|\tilde{\psi}^0(p)|^2$ values in the $0 < p \leq p_{\min}$ range, as this contribution is problematic only for the $\psi_{R\pm}(x, t)$ components, when $V_R > V_L$.

To test this assumption, we have performed $\psi_{L\pm}(x, t)$ wavepacket dynamics calculations for a second barrier ramp problem, using initial and final wavepacket conditions *identical* to Sec. III A 1—i.e., $p_0 = \sim 3.28634$ a.u. and $t_{\max} = 11600$ a.u. All other parameters are as described above. The results, presented in Fig. 7, are very similar to those of Sec. III A 1, except as expected. In particular, both components are smooth and continuous throughout, but there is a difference between $\rho(x > x_D)$ and $\rho_+(x > x_D)$, which is clearly evident at large times—even though $\rho_-(x > x_D)$ itself is barely visible. [Fig. 7(d)]. This is a further manifestation of the square-root sensitivity discussed in Sec. III A 2.

In addition to the above two barrier ramp problems, various other parameter choices have been considered, including an electron-mass version analogous to Sec. III A 3. In all cases, the resultant bipolar decompositions have been found to be well-behaved at all times.

C. Two-surface system

As our final test application, we consider a model multisurface system with $f = 2$ coupled electronic states. For this two-surface model, both of the diagonal potential energy curves, as well as the off-diagonal coupling potentials, are taken to be Eckart barriers, i.e.

$$V_{11}(x) = V_{22}(x) = V_0 \operatorname{sech}(\alpha x)^2, \quad (37)$$

$$V_{12}(x) = V_{21}(x) = D_0 \operatorname{sech}(\alpha x)^2. \quad (38)$$

In atomic units, the particular parameter values used are as follows: $V_0 = .0024$; $D_0 = .00072$; $\alpha = 2.5$; $m = 2000$; $\gamma = 0.35$; $x_0 = -7.0$; $p_0 = \sim 3.28634$. These parameters are chosen to correspond to those used in Sec. III A 1, and also to yield substantial final probability for all *four* components, $\psi_{1\pm}^f(x)$ and $\psi_{2\pm}^f(x)$.

Note that the above model system conforms to the asymptotically symmetric special case (end of Sec. II E). Consequently, the choice $V^0 = 0$ leads to perfect asymptotic separation for all four components (Condition 3).

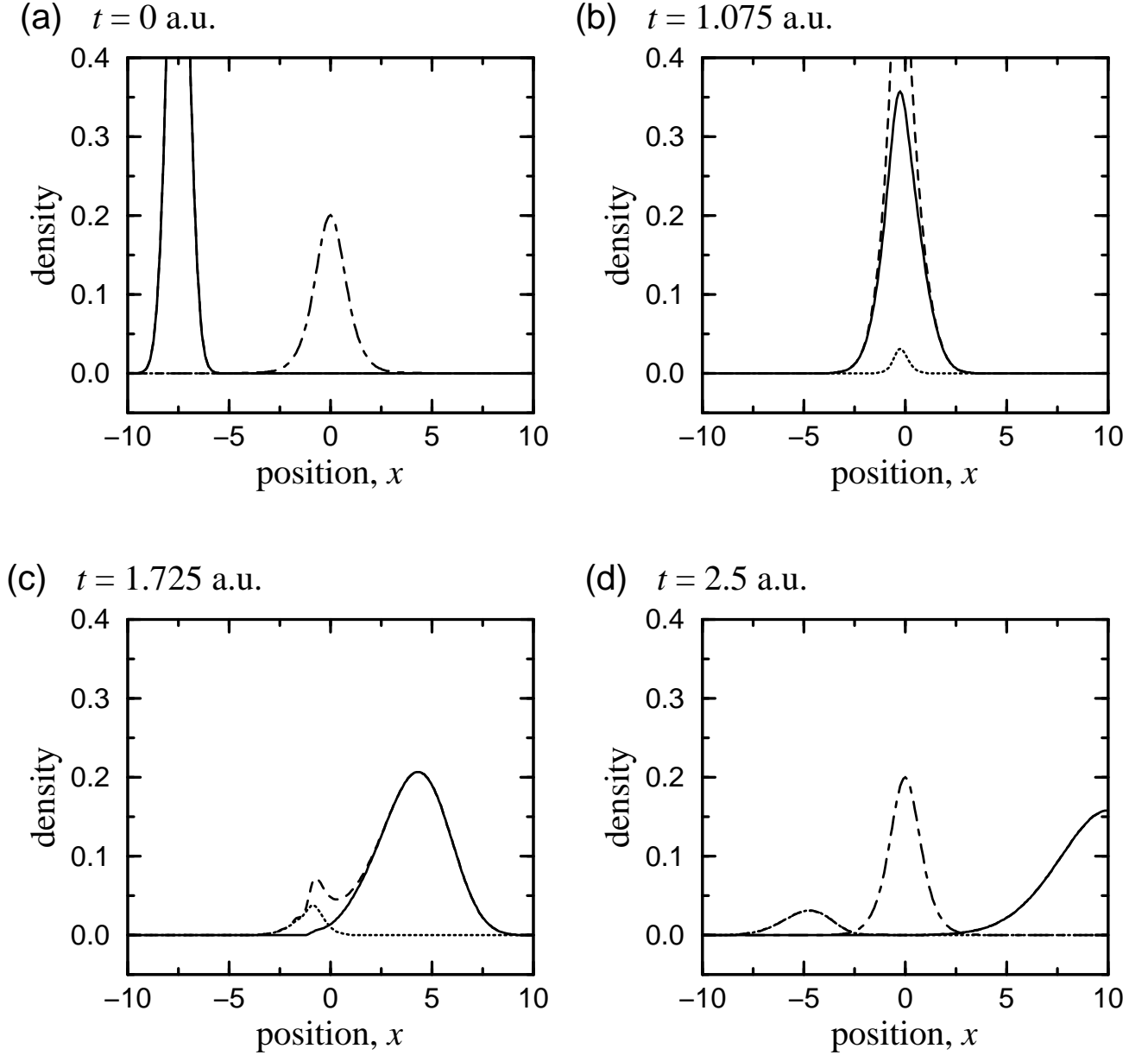


FIG. 5: Wavepacket dynamics for the symmetric Eckart barrier system with $m = 1$ a.u. Each plot represents a “snapshot” for a specific time, t , as listed (all units are atomic units). Various component wavepacket densities as a function of position are indicated; see Fig. 2 caption for explanation. In (b), the $\psi_+(x)$ peak has just passed that of $\psi_-(x)$, which is in stage 1. In (c), $\psi_-(x)$ has just entered stage 2, implying a pronounced Goos-Hänchen time delay [also suggested by (d)]. Note the evident lack of interference, and of a $\psi_+(x, t)$ spur.

Since the initial wavepacket is incident on surface $i = 1$, the only non-zero initial condition is for $\psi_{1+}^0(x)$, for which Eq. (34) is used with parameter values given above. The four components, $\psi_{1\pm}(x, t)$ and $\psi_{2\pm}(x, t)$, are then propagated using Eq. (31), to a final time $t_{\max} = 11600$ a.u. Only a single propagation is required.

Figure 8 shows the resultant multisurface wavepacket dynamics at four representative time slices. For visual clarity, the $\psi_{2\pm}(x, t)$ components are plotted above the $\psi_{1\pm}(x, t)$ —though this is *not* meant to imply that the V_{22} potential is higher in energy. From the figure, it is clear

that each of the four components is smooth and well-behaved at all x and t , and otherwise acts as expected. As the incident wave $\psi_{1+}(x, t)$ passes through the interaction region, all *three* scattered components, $\psi_{1-}(x, t)$ and $\psi_{2\pm}(x, t)$, come into being. All three of these components exhibit the two-stage process of first growing in place, and then moving away from the interaction region in their respective directions.

Note that, as in the earlier examples, $\psi_{1+}(x, t)$ develops a spur, which provides type II interference (node healing) for the “reflected” part of $\psi_1(x, t)$. The spur

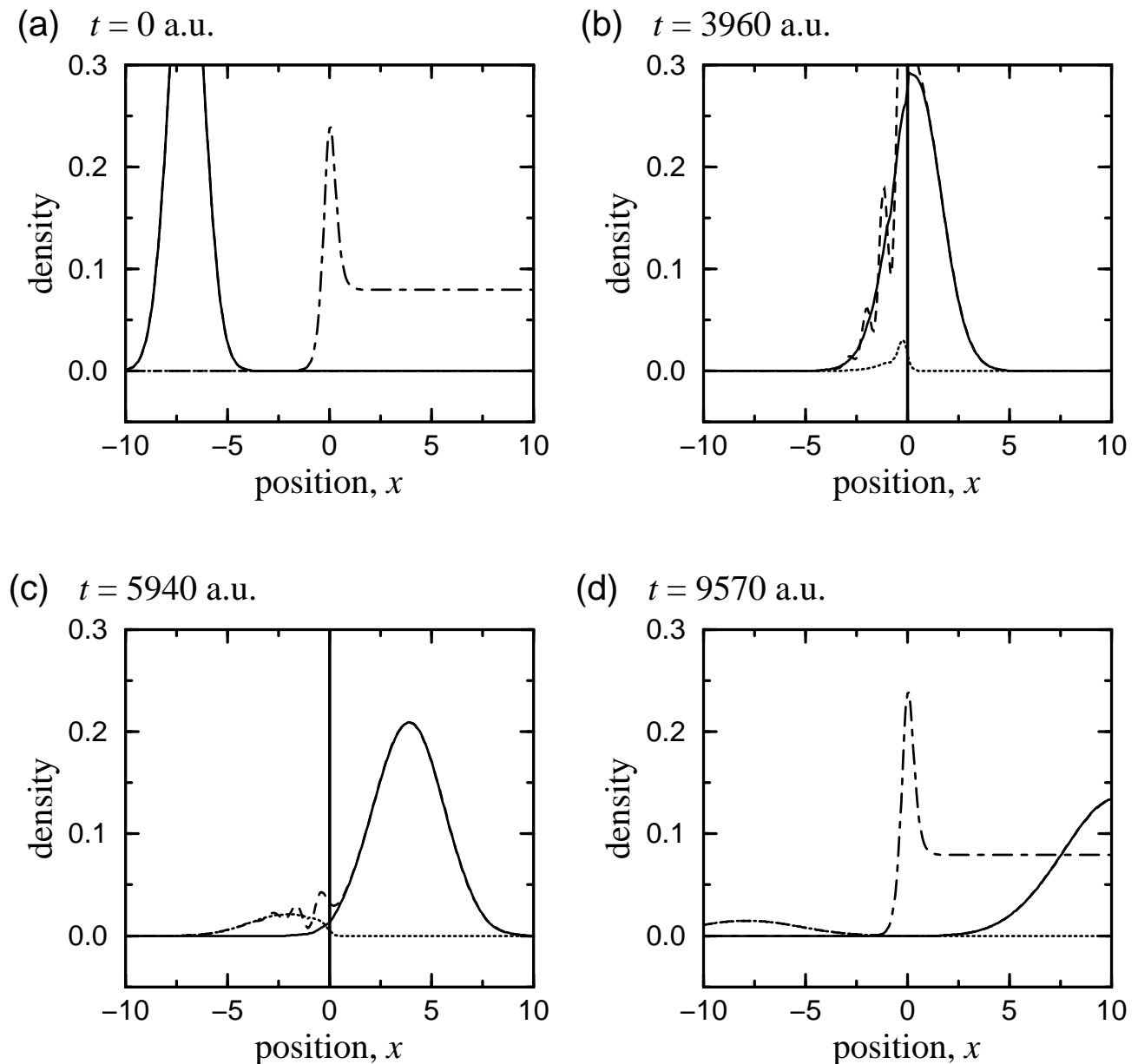


FIG. 6: Wavepacket dynamics for the asymmetric barrier ramp system using “spliced” solutions, $\psi_{\pm}(x, t)$ [Eq. (21)]. Each plot represents a “snapshot” for a specific time, t , as listed (all units are atomic units). Various component wavepacket densities as a function of position are indicated; see Fig. 2 caption for explanation. In (b) and (c), the vertical bar at $x = x_D = 0$ indicates the point where the $\psi_{L\pm}(x, t)$ and $\psi_{R\pm}(x, t)$ solutions are spliced together; the resultant discontinuity is particular evident in the $\rho_+(x)$ plot of (c) (solid curve).

is particularly prominent for this system [Fig. 8(b) and (c)]. In contrast, neither of the $\psi_{2\pm}(x, t)$ components develops a spur, so that $\psi_2(x, t)$ has no type II interference. In fact, $\psi_2(x, t)$ does not appear to exhibit any interference at all, even though the $\psi_{2\pm}(x, t)$ components do overlap slightly at intermediate times, which could in principle lead to type I interference. The reason is that the $\psi_{2\pm}(x, t)$ are both growing in place, and therefore have the same mean velocity of zero, whereas $\psi_{1+}(x, t)$ is moving relative to $\psi_{1-}(x, t)$. This situation, though easily understood within the present bipolar picture, would

perhaps be difficult to justify in purely semiclassical LM terms.

IV. SUMMARY AND CONCLUSIONS

This paper represents a turning point in the development of the bipolar QTM methodology. All of the previous papers in the series have focused exclusively on stationary states—whether bound or scattering states, for either continuous or discontinuous potentials. This

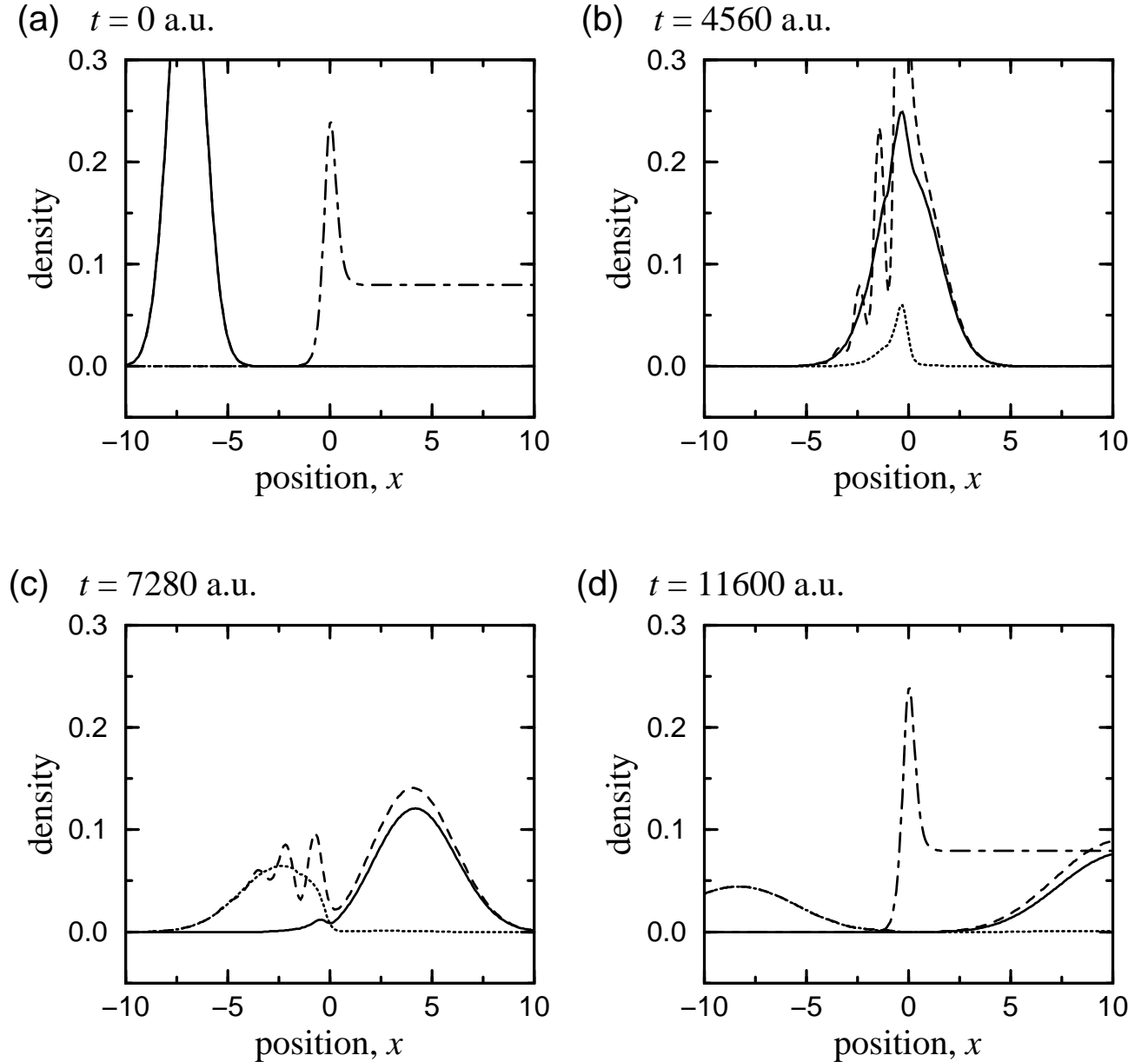


FIG. 7: Wavepacket dynamics for the asymmetric barrier ramp system using $\psi_{L\pm}(x, t)$ solutions throughout x and t . Each plot represents a “snapshot” for a specific time, t , as listed (all units are atomic units). Various component wavepacket densities as a function of position are indicated; see Fig. 2 caption for explanation. In comparison with Fig. 6, the component wavepacket densities are now continuous everywhere, but do not satisfy perfect asymptotic separation in the $(x > x_D, t_f)$ limit, as is evident in (c) and (d). Also, the reflection probability is greater, due to the smaller value of p_0 .

was a necessary prerequisite for the present paper, in addition to being useful in its own right—i.e., leading to the development of extremely efficient and robust algorithms for 1D stationary scattering applications (Ref. 27 and Ref. 30). These algorithms have been successfully applied to challenging deep tunneling applications, and also to 1D reaction path Hamiltonian approximations for real chemical reactions such as $\text{Cl}^- + \text{CH}_3\text{Cl} \rightarrow \text{ClCH}_3 + \text{Cl}^-$. On the other hand, the direct calculation of the stationary ϕ^E states, as functions of position, will never be feasible for very large systems, owing to the fact that

such states are delocalized over a configuration space of many dimensions. If such systems are to succumb to exact quantum dynamical treatment in a position-space representation, it must be via some non-stationary, localized wavepacket approach. Moreover, the dynamical equations used for the numerical wavepacket propagation must be free of any explicit dependence on the ϕ^E states, or even E itself.

This we have achieved here in Eqs. (14) and (31)—through a sequence of manipulations of the original time-evolution equations for stationary scattering states

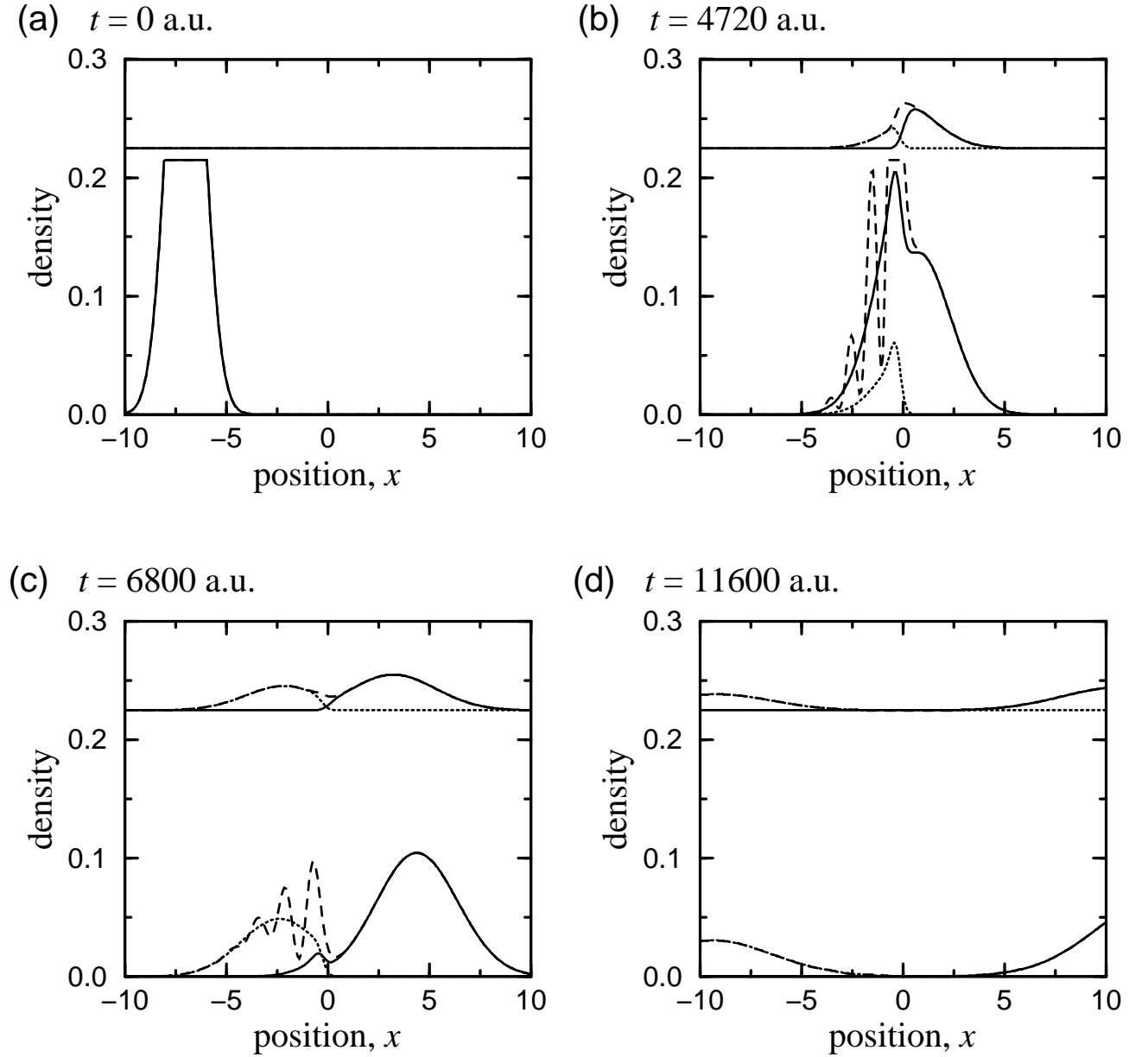


FIG. 8: Wavepacket dynamics for the symmetric multisurface application of Sec. III C. Each plot represents a “snapshot” for a specific time, t , as listed (all units are atomic units). Various component wavepacket densities as a function of position are indicated. Those for surface 1 are grouped together at the bottom of each plot as follows: incident/transmitted, $\rho_{1+}(x) = |\psi_{1+}(x)|^2$, (solid); reflected, $\rho_{1-}(x) = |\psi_{1-}(x)|^2$, (dotted); total, $\rho_1(x) = |\psi_1(x)|^2$, (dashed). The corresponding surface 2 densities are grouped at the top of each plot in similar fashion—e.g., transmitted, $\rho_{2+}(x) = |\psi_{2+}(x)|^2$, via the upper solid curve, etc. Surface 2 exhibits little or no interference, in part due to a lack of spurs. In contrast, the $\psi_{1+}(x, t)$ spur is quite pronounced at intermediate times, i.e. in (b) and (c).

[Eq. (3)], and the introduction of reasonable restrictions on the allowed wavepacket dynamics (Sec. II C). The intermediate result, Eq. (10), though not used directly, depends on the JWKB quantity (Sec. II B)—thereby affording a theoretical connection with semiclassical mechanics and the classical limit. The final Eq. (14) is an integro-differential equation that depends on the spatial *integral* of ψ_{\pm} , rather than the integral of $|\psi_{\pm}|^2$, or ψ_{\pm} itself. This is quite unusual in the context of quantum

dynamics—though commonplace, for instance, in soliton dynamics.^{46,47} In any case, it is precisely this spatial integration that removes all explicit dependence of Eq. (13) on E and p —the crucial requirement in the derivation of Eq. (14).

The derivation is more involved than originally anticipated, owing to the fact that Eq. (3) is presented in a form that is unsuitable for a wavepacket generalization—even though ultimately, Eq. (14) is derived from Eq. (3),

and is thus equivalent to it (at least at asymptotically large times). Nevertheless, there are essential differences between the two equations, stemming from the fact that the coupling contribution in Eq. (3) is not the same as in Eq. (13). One important difference is that Eq. (14) is independent of the constant potential value, V_0 , used to define the stationary state trajectories (though the V_0 value does affect the initial value conditions). Also, the TDSE is satisfied at all times (not just asymptotically large times). Finally, unlike Eq. (3), Eq. (14) does not conserve total integrated probability [Eq. (17)].

Another important new development is that the bipolar wavepacket methodology readily lends itself to a traditional Bohmian mechanics interpretation—e.g., quantum trajectories defined via $S'_\pm = p_\pm$ [Eq. (18)], with dynamics governed by the quantum potential. The behavior of the bipolar quantum trajectories ensuing from Eq. (14) will be explored in a future publication. In practical terms, however, the trajectories are essentially guaranteed to be well-behaved, provided that all three of the conditions for well-behaved bipolar wavepacket components, as described in Sec. II C, are satisfied for all x and t . Condition 3., in particular, is required to circumvent the node problem plaguing the synthetic QTM approach, and is therefore essential for application to large systems, for which the Eulerian fixed-grid algorithm used here (however efficiently implemented) would be unfeasible.

To satisfy all three conditions of Sec. II C for a wide variety of applications is decidedly nontrivial, and quite a lot to ask of any set of dynamical equations—especially with regard to the interference Condition 3., owing to the square-root sensitivity discussed in Sec. III A 2. Indeed, it may be the case that *no* set of evolution equations other than Eq. (14) would be capable of achieving such a separation for general applications. In fact, a great many candidates were explored and rejected, for failing to satisfy Condition 3 (and in many cases, Conditions 1. and 2. as well).²⁹ The examples of Sec. III (and others) nevertheless indicate that the present bipolar wavepacket approach appears capable of achieving this—in both the quantum and classical limits, and even when there is a complicated interplay of at least two different types of interference. These examples also clearly demonstrate that virtually all quantum effects that play a role in wavepacket dynamics—i.e. dispersion, tunneling, and interference—can be easily incorporated. Note that for real molecular systems with atomic nuclei heavier than hydrogen, interference effects can be even more pronounced than for any of the examples considered in this paper; such cases will be considered in future publications.

The present work thus serves to demonstrate that a synthetic bipolar wavepacket QTM approach based on Eq. (14) would be widely applicable and numerically feasible—using the quantum potential to handle those quantum effects that it does best, i.e. dispersion and tunneling, and intercomponent coupling to treat inter-

ference. The numerical algorithm would employ well-established unstructured grid techniques, such as local least-squares fitting,^{11,16,48} that have already been applied successfully to standard unipolar wavepacket QTM applications *without* interference. In the unipolar context, the chief numerical requirement is the calculation of spatial derivatives needed to compute the quantum potential or quantum force. The only new numerical requirement for the bipolar treatment is that of spatial *integration*, to evaluate $\Psi_\pm(x, t)$ at every time step. This is not anticipated to pose severe numerical difficulties, even for multidimensional applications, as the generalization of Eq. (15) is a *line* integral (1D), rather than a volume integral over all degrees of freedom.

As a practical matter, it is important that the present approach can be generalized for arbitrary asymmetric potentials, and even multisurface applications, as discussed in Secs. II D and II E, respectively. Intriguingly the time-evolution equations for the former are unmodified from the symmetric case, although the initial and final value conditions do depend on the asymptotic potential values. From a formal perspective, the fact that multiple calculations must be performed in the asymmetric case—and then “glued” together discontinuously at the dividing point, x_D —is perhaps less appealing than the continuous V^{eff} approach developed for stationary state applications in Ref. 30. On the other hand, the discontinuous approach is also taken by other standard “dividing surface” reactive scattering methods, which essentially posit two completely different asymptotic Hamiltonians, one for reactants, and one for products.^{34,35} In any event, a generalization of the bipolar wavepacket theory using step effective potentials $V^{\text{eff}}(x) = V_L + (V_R - V_L)\Theta(x - x_D)$ directly (Ref. 26), will be explored in a future paper. This will allow direct propagation across the discontinuity, which in turn, implies that only a single calculation need be performed for asymptotically asymmetric systems, while still satisfying perfect asymptotic separation. Another issue that may be considered in future is the generalization for initial wavepackets that do *not* satisfy Eq. (16)—i.e., that include an initially outgoing contribution. The nominal difficulty is that such wavepackets lead to delocalized Ψ functions, although this issue may be resolved by explicit consideration of the *right*-incident stationary solutions.

In addition to the various “horizontal” developments, to be considered in future publications as described above, the next step in the “vertical” or methodological direction—and the subject of the final paper in this series—remains the development of a *multidimensional* generalization. In a sense, Eq. (31) already provides one avenue for multidimensional application—in that the multiple surfaces may be regarded as parametrized, discrete quantum states for all of the “perpendicular” degrees of freedom. This approach could be used, for instance, to treat rotational degrees of freedom in the context of a partial wave expansion. In paper VI though, we shall address wavepacket dynamics directly on the

full-dimensional configuration space. The theoretical development required will be seen to be a remarkably straightforward generalization of that presented here. In particular, only *two* wavefunction components are still required—regardless of system dimensionality—provided there is a single reaction path. Moreover, the formalism can accommodate standard Jacobi-type coordinate representations with arbitrary curvilinear reaction paths. Paper VI will present results for several multidimensional applications including collinear H+H₂—the first such exact quantum dynamics calculations ever performed using a QTM. Moreover, the resultant multidimensional ψ_{\pm} decomposition will be found to satisfy the three all-important conditions of Sec. II C.

As a final observation, we note that the bipolar wavepacket decomposition as presented in this paper is by no means restricted to the Bohmian mechanics context only. More generally, it ought to be regarded as a scattering formalism in its own right, which could in principle impact favorably on any of a number of existing computational methodologies. Even straightforward Eulerian fixed-grid propagations, for instance, might benefit from the greatly increased grid spacing and time step sizes associated with the component $\psi_{\pm}(x, t)$'s—which are much smoother in general than $\psi(x, t)$ itself, particularly in the classical limit. Another idea might

be to exploit the Gaussian-like properties of the component $\psi_{\pm}(x, t)$'s to develop an approximate Gaussian evolution scheme, à la Heller.^{1,49} Perhaps as few as three such “growing Gaussians” would be required—one for the incident/transmitted wavepacket, one for the reflected wavepacket, and a third for the spur.

Acknowledgments

This work was supported by a grant from The Welch Foundation (D-1523), and by a Small Grant for Exploratory Research from the National Science Foundation (CHE-0741321). The author wishes to express gratitude to Yair Goldfarb, Salvador Miret-Artés, Lucas Pettey, Angel Sanz, David Tannor, and Robert Wyatt, for many interesting discussions. The author is particularly indebted to George Hinds and Jeremy Schiff for discussions pertaining to the possible relationship between quantum dynamics and solitons. Lucas Pettey, and especially Corey Trahan are also acknowledged, for Herculean efforts to implement a great many of the earlier, unsuccessful ideas. Jason McAfee is also acknowledged for his aid in converting this manuscript to an electronic format suitable for the arXiv preprint server.

* Electronic address: Bill.Poirier@ttu.edu

- ¹ D. J. Tannor, *Introduction to Quantum Mechanics: A Time-Dependent Perspective* (University Science Books, Sausalito, 2007).
- ² N. Fröman and P. O. Fröman, *JWKB Approximation* (North-Holland, Amsterdam, 1965).
- ³ M. V. Berry and K. V. Mount, *Rep. Prog. Phys.* **35**, 315 (1972).
- ⁴ E. Madelung, *Z. Phys.* **40**, 322 (1926).
- ⁵ D. Bohm, *Phys. Rev.* **85**, 166 (1952).
- ⁶ D. Bohm, *Phys. Rev.* **85**, 180 (1952).
- ⁷ P. R. Holland, *The Quantum Theory of Motion* (Cambridge University Press, Cambridge, 1993).
- ⁸ H. Wu and D. W. L. Sprung, *Phys. Lett. A* **183**, 413 (1993).
- ⁹ A. S. Sanz, F. Borondo, and S. Miret-Artés, *J. Phys. Condens. Matter* **14**, 6109 (2002).
- ¹⁰ Z. S. Wang, G. R. Darling, and S. Holloway, *J. Chem. Phys.* **115**, 10373 (2001).
- ¹¹ R. E. Wyatt, *Quantum Dynamics with Trajectories: Introduction to Quantum Hydrodynamics* (Springer, New York, 2005).
- ¹² C. L. Lopreore and R. E. Wyatt, *Phys. Rev. Lett.* **82**, 5190 (1999).
- ¹³ F. S. Mayor, A. Askar, and H. A. Rabitz, *J. Chem. Phys.* **111**, 2423 (1999).
- ¹⁴ D. V. Shalashilin and M. S. Child, *J. Chem. Phys.* **113**, 10028 (2000).
- ¹⁵ R. E. Wyatt, C. L. Lopreore, and G. Parlant, *J. Chem. Phys.* **114**, 5113 (2001).
- ¹⁶ R. E. Wyatt and E. R. Bittner, *J. Chem. Phys.* **113**, 8898 (2001).
- ¹⁷ C. L. Lopreore and R. E. Wyatt, *J. Chem. Phys.* **116**, 1228 (2002).
- ¹⁸ E. R. Bittner, J. B. Maddox, and I. Burghardt, *Int. J. Quantum Chem.* **89**, 313 (2002).
- ¹⁹ K. H. Hughes and R. E. Wyatt, *Phys. Chem. Chem. Phys.* **5**, 3905 (2003).
- ²⁰ D. Babyuk and R. E. Wyatt, *J. Chem. Phys.* **121**, 9230 (2004).
- ²¹ C. J. Trahan and R. E. Wyatt, *J. Chem. Phys.* **118**, 4784 (2003).
- ²² B. K. Kendrick, *J. Chem. Phys.* **119**, 5805 (2003).
- ²³ D. K. Pauler and B. K. Kendrick, *J. Chem. Phys.* **120**, 603 (2004).
- ²⁴ B. Poirier, *J. Chem. Phys.* **121**, 4501 (2004).
- ²⁵ C. Trahan and B. Poirier, *J. Chem. Phys.* **124**, 034115 (2006).
- ²⁶ C. Trahan and B. Poirier, *J. Chem. Phys.* **124**, 034116 (2006).
- ²⁷ B. Poirier and G. Parlant, *J. Phys. Chem. A* **111**, 10400 (2007).
- ²⁸ L. Pettey, B. Poirier, and R. E. Wyatt (unpublished).
- ²⁹ C. Trahan and B. Poirier (unpublished).
- ³⁰ B. Poirier, *J. Theo. Comput. Chem.* **6**, 99 (2007).
- ³¹ B. Poirier, *Phys. Rev. A* (2007), (in press).
- ³² G. Bertoldi, A. E. Faraggi, and M. Matone, *Class. Quantum Grav.* **17**, 3965 (2000).
- ³³ R. Liboff, *Introductory Quantum Mechanics*, 1st ed. (Holden-Day, Inc., Oakland, CA, 1980).
- ³⁴ T. Seideman and W. H. Miller, *J. Chem. Phys.* **96**, 4412 (1992).

- ³⁵ N. Rom, N. Moiseyev, and R. Lefebvre, *J. Chem. Phys.* **96**, 8307 (1992).
- ³⁶ W. H. Press *et al*, in *Numerical Recipes*, 1st ed. (Cambridge University Press, Cambridge, England, 1989).
- ³⁷ See EPAPS Document. No. xxx for computer animations (.wmv file format) for all of the wavepacket dynamics calculations presented in this paper. This document can be reached through a direct link in the online article's HTML reference section or via the EPAPS homepage (<http://www.aip.org/pubservs/epaps.html>).
- ³⁸ C. Eckart, *Phys. Rev.* **35**, 1303 (1930).
- ³⁹ Z. Ahmed, *Phys. Rev. A* **47**, 4761 (1993).
- ⁴⁰ J. O. Hirschfelder, A. C. Christoph, and W. E. Palke, *J. Chem. Phys.* **61**, 5435 (1974).
- ⁴¹ J. D. Jackson, *Classical Electrodynamics*, 2nd ed. (John Wiley & Sons, New York, 1975).
- ⁴² J. B. Keller and S. I. Rubinow, *Ann. Phys.* **9**, 24 (1960).
- ⁴³ V. P. Maslov, *Théorie des Perturbations et Méthodes Asymptotiques* (Dunod, Paris, 1972).
- ⁴⁴ D. Huber, E. J. Heller, and R. G. Littlejohn, *J. Chem. Phys.* **89**, 2003 (1988).
- ⁴⁵ R. G. Littlejohn, *J. Stat. Phys.* **68**, 7 (1992).
- ⁴⁶ T. Dauxois and M. Peyrard, *Physics of Solitons* (Cambridge University Press, Cambridge, 2006).
- ⁴⁷ J. Schiff, (private communication).
- ⁴⁸ R. E. Wyatt, *Chem. Phys. Lett.* **313**, 189 (1999).
- ⁴⁹ E. J. Heller, *J. Chem. Phys.* **75**, 2923 (1981).